Title: ATRAID, a genetic factor that regulates the clinical action of nitrogen-containing bisphosphonates on bone

Authors: Lauren E. Surface[1], Jiwoong Park[2], Sandeep Kumar[2], Damon T. Burrow[2], Cheng Lyu[2], Jinmei Li[2], Niki Song[2], Zhou Yu[1], Abbhirami Rajagopal[3,#], Yangjin Bae[3], Brendan H. Lee[3], Steven Mumm[4], Gabe Haller[5], Charles C. Gu[6], Jonathan C. Baker[7], Mahshid Mohseni[4], Melissa Sum[8], Margaret Huskey[4], Shenghui Duan[4], Vinieth N. Bijanki[9], Roberto Civitelli[4], Michael J. Gardner[10], Chris M. McAndrew[5], William M. Ricci[5], Christina A. Gurnett[5], Kathryn Diemer[4], Michael P. Whyte[4,9], Jan E. Carette[11], Malini Varadarajan[12,*], Thijn R. Brummelkamp[12], Kivanc Birsoy[13], David M. Sabatini[14-16], Erin K. O'Shea[17], Timothy R. Peterson[2]

Affiliations:

[1] Department of Molecular and Cellular Biology, Department of Chemistry and Chemical Biology, Faculty of Arts and Sciences Center for Systems Biology, Harvard University, Cambridge, MA 02138, USA.

[2] Division of Bone & Mineral Diseases, Department of Internal Medicine, Department of Genetics, Institute for Public Health, Washington University School of Medicine, BJC Institute of Health, 425 S. Euclid Ave., St. Louis, MO 63110, USA.

[3] Department of Molecular and Human Genetics, Baylor College of Medicine, Houston, TX, 77030, USA.

[#] (present address) Harris County Public health, Houston, TX, 77027, USA.

[4] Division of Bone & Mineral Diseases, Department of Internal Medicine, Washington University School of Medicine, BJC Institute of Health, 425 S. Euclid Ave., St. Louis, MO 63110, USA.

[5] Department of Orthopedic Surgery, Washington University School of Medicine, 4938 Parkview Place, St. Louis, MO 63110, USA.

[6] Division of Biostatistics, Washington University School of Medicine, 660 S. Euclid Ave., CB 8067, St. Louis, MO 63110-1093, USA.

[7] Mallinckrodt Institute of Radiology, Washington University School of Medicine, 510 S. Kingshighway Blvd. Louis, MO 63110, USA.

[8] Division of Endocrinology, Diabetes and Metabolism, NYU Langone Health, 530 1st Ave., Schwartz 5E. New York, NY 10016, USA.

[9] Center for Metabolic Bone Disease and Molecular Research, Shriners Hospital for Children, St. Louis, MO 63110, USA.

[10] Stanford University, Department of Orthopedic Surgery, 450 Broadway Street, Redwood City, CA 94063-6342, USA.

[11] Department of Microbiology and Immunology, Stanford University School of Medicine, Stanford, CA 94305, USA.

[12] Netherlands Cancer Institute, Amsterdam, The Netherlands.

[*] (present address) Developmental and molecular pathways, Novartis institutes for biomedical research, Cambridge, CA 02140, USA.

[13] The Rockefeller University, 1230 York Ave, New York 10065, USA.

[14] Whitehead Institute, 9 Cambridge Center, Cambridge, MA 02139, USA.

[15] Department of Biology, Massachusetts Institute of Technology (MIT), 77 Massachusetts Avenue, Cambridge, MA 02139, USA.

[16] David H. Koch Center for Integrative Cancer Research at MIT, 77 Massachusetts Avenue, Cambridge, MA 02139, USA.

[17] Howard Hughes Medical Institute, 4000 Jones Bridge Road, Bethesda, MD 20815, USA.

* Correspondence to: osheae@hhmi.org (E.K.O.), timrpeterson@wustl.edu (T.R.P).

One Sentence Summary: The identification of the gene, *ATRAID*, essential for responses to the commonly prescribed osteoporosis (i.e., bone loss) drugs, nitrogen-containing bisphosphonates.

Abstract:

Nitrogen-containing bisphosphonates (N-BPs), such as alendronate (Fosamax®), are the mostly widely prescribed medications for diseases involving bone[1-3], with nearly 200 million prescriptions written annually. In the last few years, widespread use of N-BPs has been challenged due to the risk of rare but significant side effects such as atypical femoral fractures and osteonecrosis of the jaw[4-7]. N-BPs bind to and inhibit farnesyl diphosphate synthase (FDPS), resulting in defects in protein prenylation[8-10]. Yet it remains poorly understood what other cellular targets N-BPs might have. Herein, we perform genome-wide studies in cells and patients to identify the gene, *ATRAID*, that functions with FDPS in a novel pathway we name the TBONE (Target of Bisphosphonates) pathway. Loss of *ATRAID* function results in selective resistance to N-BP-mediated loss of cell viability and the prevention of alendronate-mediated inhibition of prenylation. *ATRAID* is required for alendronate inhibition of osteoclast function, and *ATRAID*-deficient mice have impaired therapeutic responses to alendronate in a model of postmenopausal osteoporosis. Our work adds key insight into the mechanistic action of N-BPs and the processes that might underlie differential responsiveness to N-BPs in people.

Nitrogen-containing bisphosphonates (N-BPs) are the standard treatment for osteoporosis and several other bone diseases[11,12]. Certain N-BPs (pamidronate (Aredia®), zoledronate (Zometa®)) are also routinely prescribed to prevent skeletal complications in patients with multiple myeloma and with bone metastases from other malignancies, including breast and prostate cancer[13]. However, because N-BPs cause rare yet serious side-effects, such as atypical fractures and osteonecrosis of the jaw, many patients avoid taking them[5-7,11], causing the number of prescriptions to plummet over 50% in the last decade[7,14]. Thus, there is a sizeable and growing need to better understand the genetic factors that might underlie the on- and off-target clinical effects of the N-BPs.

A goal of personalized medicine is to identify biomarkers that underlie drug responsiveness. In the case of the N-BPs, it can be said that there are limited personalization options owing to the limited number of genes implicated in the mechanism of action of N-BPs on bone. Exposure of cells to N-BPs leads to inhibition of farnesyl pyrophosphate synthase (FDPS, a.k.a., FPPS) resulting in reduction in protein prenylation[15]. Based on this observation, it is widely believed that N-BPs act therapeutically by impairing protein prenylation, ultimately leading to deficits in numerous cellular processes including differentiation, recruitment, and adhesion of osteoclasts (the major bone resorptive cell type) to bone and/or osteoclast cell death[16-18]. Major open questions remain regarding how N-BPs inhibit FDPS in osteoclasts. Namely, because N-BPs are highly charged molecules, it is unclear what genes may be required for internalizing and transporting N-BPs to allow them access to FDPS. N-BPs may also influence osteoblasts[19,20], the major bone matrix depositing cell type[21], and osteocytes[22] though many of these studies were done in cell culture with a question of how the doses used would compare to the *in vivo* exposure[23,24]. One complication is that any *in vivo* effect of N-BPs on osteoblasts may be attributable to indirect effects on the bone remodeling cycle caused by the reduction in bone resorption and consequent reduction in bone formation[24]. Thus, in numerous ways our

understanding of the molecular mechanisms by which N-BPs regulate the major bone cell types would be improved by further studies.

To provide insight into the mechanism(s) of N-BPs action, we performed a genetic screen to identify human genes required for the anti-proliferative effects of N-BPs (Fig. 1a). We made use of a largely haploid human cell line of myeloid origin (KBM7, a.k.a. HAP1) to generate a library of retroviral gene trap mutants[25], and then selected for clones which are resistant to cytotoxic levels of alendronate. The advantages of this cell line for genetic screening include: 1) each gene is present as a single copy, enabling gene inactivation (except those genes on chromosome 8); and 2) KBM7 cells are human and of the hematopoietic lineage, increasing the likelihood that any genes we identify could be relevant to the natural context for N-BPs, the bones of human patients[26]. Using this haploid approach, we identified a poorly characterized gene, *ATRAID*, a.k.a., *APR3/C2orf28*[27], as the gene most significantly enriched for insertions in alendronate resistant cells compared to untreated cells (Fig. 1b, and Supplementary Table 1a).

Other genes identified in our alendronate haploid screen (*SNTG1*, *PLCL1*, and *EPHB1)* have been previously connected to N-BP action on bone cells and/or human bone diseases[28-30]. To systematically evaluate all “hits” we identified (i.e., the 185 genes with FDR p-value < 0.05, see Fig. 1b), we developed a computational approach utilizing a molecular biology-optimized version of PubMed (currently at ~27M records) to assess to what extent our haploid screen identified genes were cited as relevant to human studies that focus on bone (see “PubMed citation analysis” in the Methods section for details). We asked whether our alendronate haploid screen hits were mentioned in publications co-occurring with the term “bone” vs. other tissues along with identifiers of genome-wide screening, namely the strings, “GWAS” or “genome-wide” (Fig. 1c). Indeed, our alendronate screen hits were enriched in publications co-mentioning “bone” and genome-wide studies compared to control gene sets (Fig. 1d, Supplementary Table 1b). This

suggests that the KBM7 cells we used and our screening approach with alendronate can identify genes relevant to human bone.

N-BPs target FDPS in the mevalonate, a.k.a. cholesterol biosynthesis, pathway (Fig. 1e). The statins, which are cholesterol lowering drugs for heart health[31], are a widely used drug class that, like the N-BPs, target the mevalonate pathway (Fig. 1e). Therefore, it seemed possible that *ATRAID* and other genes we identified with alendronate in our haploid screen might also score highly with statins. In haploid screening for genes which when inactivated conferred resistance to two statins, simvastatin and lovastatin (a.k.a., mevinolin), we didn't detect *ATRAID*, though we did identify several novel factors including *WT1* that were common to both statins (Fig. 1f, Supplementary Table 1a). Because *FDPS* is essential[32-34], and thus wouldn't be detected with our haploid approach, we employed a knockdown-based approach, CRISPRi[35] as a complementary strategy (Fig. 1g). Using CRISPRi, we identified both *ATRAID* and *FDPS* among the top 200 hits with alendronate[36], but not with several other clinical and experimental drugs including ones that regulate the mevalonate pathway (Fig. 1h and Supplementary Table 1a)[37-39]. Taken together with our haploid screening and recent work on *FDPS* by Horlbeck et al.[40], this data suggests *ATRAID* and *FDPS* might be part of a unique pathway separable from that targeted by the statins and other drugs.

These genome-wide screens were in cells, so we sought to test whether the genes we identified might be relevant in patients treated with N-BPs. We performed exome sequencing of osteoporotic patients who experienced atypical femoral fractures (AFF) when taking N-BPs and compared their DNA with osteoporotic patients who didn't suffer this side effect (Fig. 1i). We also analyzed two published gene expression datasets involving patients who had taken N-BPs: multiple myeloma patients who did or did not suffer osteonecrosis of the jaw (ONJ) when taking N-BPs[41]; and breast cancer patients with bone marrow disseminated tumor cells (DTC) which

reoccurred or the patient died less than 1000 days vs. greater than 2500 days following initiation of zolendronate treatment[42] (Fig. 1i, and Supplementary Fig. 1c). In comparing our cell-based CRISPRi screen with the three patient-based datasets, *ATRAID* was amongst the 30 genes that scored in all datasets (Fig. 1j and k). *FDPS* and *IDI1,* which produces a metabolite, dimethylallylpyrophosphate (DMAPP) required for the synthesis of the major FDPS product, farnesyl pyrophosphate (FPP), were also differentially expressed and/or possessed coding variants only seen in the poor N-BP treatment outcome arms of several of the patient datasets (Fig. 1k and Supplementary Fig. 1). Taken together, this suggests that *FDPS* and the novel factor, *ATRAID*, may influence N-BP responses in people.

Recently we identified another gene, *SL37A3*, that provides molecular details for how *ATRAID* connects to the N-BPs and FDPS[36]. However, because *SLC37A3* wasn't amongst the 30 genes that scored in all the patient- and cell-based studies (Fig. 1i, j), we focused our further characterization on *ATRAID*. *ATRAID* was originally identified as a gene whose mRNA expression is strongly induced by the ligand, all-trans retinoic acid[27]. *ATRAID* is conserved in chordates and contains a signal peptide, Toll-like-receptor leucine rich repeat, EGF-like domain, and a transmembrane domain (Fig. 2a and Supplementary Fig. 2a)[43,44]. Importantly, the alendronate resistance phenotype of *ATRAID* deficient cells (ATRAID_GT1 (gene-trap1) and ATRAID_GT2 (gene-trap2)) was reversed by the re-introduction of wild-type *ATRAID* splice variant 2 (v2) or splice variant 3 (v3) cDNA, which differ in their N-termini (Fig. 2b, Supplementary Fig. 2a, b). To better understand the level of alendronate resistance in *ATRAID* deficient cells, we varied both cell number and drug concentration in the viability assay. *ATRAID* deficient cells were resistant to alendronate over two to three orders of magnitude of drug concentration or cell number (Supplementary Fig. 2c). Overexpression of full-length *ATRAID* (v2) sensitized cells to alendronate (Supplementary Fig. 2d). Lastly, ATRAID membrane targeting is required for the anti-proliferative effects of alendronate, as *ATRAID* deficient cells

complemented with full-length ATRAID (v2) were sensitive to the cytotoxic effects of alendronate, whereas those expressing the membrane truncated form remained resistant (Supplementary Fig. 2e). Taken together, these data establish *ATRAID* as a genetic factor required for the growth inhibitory effects of alendronate.

N-BPs are part of a larger class of compounds known as bisphosphonates (BPs) that contain two phosphate moieties each joined to a carbon atom by a carbon-phosphorus bond[45] (Fig. 2c). To determine whether the effects of *ATRAID* deficiency on alendronate resistance were specific to nitrogen-containing bisphosphonates, we tested the effect of several nitrogen-containing and non-nitrogen-containing bisphosphonates on wild-type and mutant *ATRAID* cells. Strikingly, *ATRAID* deficient cells were resistant to all nitrogen-containing bisphosphonates tested including alendronate, zoledronate, ibandronate and pamidronate, but were as sensitive to the non-nitrogen-containing bisphosphonates, etidronate and tiludronate, as control cells (Fig. 2d). Consistent with our haploid statin screens (Supplementary Fig. 1a and Supplementary Table 1a), *ATRAID* deficient cells were not resistant to the statin, lovastatin (Fig. 2e). The lack of resistance of *ATRAID*-deficient cells to non-nitrogen-containing bisphosphonates and lovastatin suggests that the effects we observe are specific to nitrogen-containing bisphosphonates. This specificity is consistent with the observation that non-nitrogen-containing bisphosphonates and nitrogen-containing bisphosphonates have distinct mechanisms of action[45].

To determine whether *ATRAID* is required for the reduction in protein prenylation observed upon N-BP treatment, we monitored the prenylation of several proteins, including the heat shock protein DnaJ (Hsp40) homolog HDJ-2, and the Ras family GTPase Rap1a[46]. Alendronate strongly inhibited prenylation of HDJ-2 and Rap1a in wild-type cells in a dose dependent manner, and had much less of an effect on prenylation of these proteins in *ATRAID*-deficient cells (Fig. 2f). Furthermore, the inhibitory effect of alendronate on prenylation was rescued when

ATRAID cDNA variants (v2 and v3) were introduced (Supplementary Fig. 2f). We observed inhibition of prenylation resistance at N-BP doses where we did not see PARP-1 cleavage in *ATRAID* deficient cells, suggesting that *ATRAID* can mediate the effect on prenylation independent of apoptosis (Supplementary Fig. 2f). Thus, *ATRAID* functions upstream of *FDPS* and in total, these findings suggest that *ATRAID* is required for molecular responses to N-BPs.

N-BPs can affect numerous cell types when administered to intact mammals, therefore to evaluate the role of *ATRAID* in N-BPs responses, we inactivated *ATRAID* globally in mice[47]. We confirmed deletion of *ATRAID* exons 3-5 and determined that *ATRAID* homozygous deleted *ATRAID*^{KO} mice (labeled KO, -/-) are viable but their body weight is mildly reduced compared with litter-matched derived, wild-type controls (labelled as WT, +/+) (Supplementary Fig. 3a-c). We confirmed that tail fibroblasts derived from *ATRAID*^{KO} animals are resistant to the cytotoxic effects of alendronate (Supplementary Fig. 3d, e).

Before studying the effects of the N-BPs in the context of *ATRAID* loss, we first characterized the basal role of *ATRAID* in bones. We determined that *ATRAID* mRNA expression was undetectable in the bones of *ATRAID*^{KO} animals and that *ATRAID*^{KO} mice had slightly smaller bones compared with litter-matched derived, wild-type control mice (Supplementary Fig. 3f, g). To examine the effects of *ATRAID* on bone structure, we performed micro-computed tomography (μCT) analysis[48]. *ATRAID* deficiency did not significantly decrease either trabecular and cortical structural parameters (Supplementary Fig. 3h, i). We measured bone strength using three-point bending tests[49]. Some measures, such as stiffness (Newtons/meter, N/m) and post-yield displacement (a measure of bone fragility, in millimeters, m) were decreased by *ATRAID* deficiency, whereas others such, as yield load (the point where bone bending goes from elastic vs. plastic, in Newtons, N), were not significantly altered (Supplementary Fig. 3j-l).

Osteoclasts release degradation products from C-terminal telopeptides of type I collagen (CTX-I) from bone into blood[50], and levels of CTX-I in serum were unchanged in wild-type mice compared with *ATRAID*^{KO} mice (Supplementary Fig. 3m). Histomorphometric measures of osteoclast function including osteoclast surface per bone surface (Oc.S/BS)[51], as judged by Tartrate Acid Resistant Phosphatase TRAP staining[52], were also unchanged (Supplementary Fig. 3n). Consistent with basal defects in osteoblast function, *ATRAID*^{KO} mice have reduced serum levels of circulating Gla-Osteocalcin (Gla-OC; the activated form of OC, incorporated in bone matrix[53]) and modestly reduced bone formation rate (BFR) as measured by double-labeling[51] (Supplementary Fig. 3o, p).

To test the effect of alendronate in a model that mimics menopausal bone loss, the most common indication for the N-BPs, we performed ovariectomies (OVX) on adult female mice (Fig. 3a)[54]. When ovaries are removed from females, the changes in estrogen cause a reduction in bone density triggered by disruption of the balance of osteoblast and osteoclast functions. This loss of bone density can be alleviated by treatment with N-BPs[55]. The magnitude of trabecular bone loss in WT and *ATRAID*^{KO} sham mice four weeks after OVX is exemplified in the μCT 3D reconstruction of the femoral proximal metaphysis (Fig. 3b). In wild-type mice, we found decreased bone density as measured by femoral cortical and trabecular structural parameters, including cortical thickness and bone volume/trabecular volume (%), after OVX compared to the sham group, (Fig. 3c, d and Supplementary Fig. 3q, s, see WT +/- OVX)[55]. Consistent with alendronate preventing bone loss, femoral structural parameters were increased by alendronate treatment of WT OVX mice (Fig. 3b-d See WT OVX +/- alendronate). In contrast, alendronate had blunted effects in *ATRAID*^{KO} OVX mice (Fig. 3b-d and Supplementary Fig. 3q, r, see *ATRAID*^{KO} OVX +/- alendronate). The same patterns of resistance in *ATRAID* KO mice were observed for both bone strength and serum bone proteins (Fig. 3e-i). That is, alendronate increased bone strength as judged by stiffness and yield load and decreased

biochemical markers of bone turnover, CTX-I and total osteocalcin (OC), in wild-type ovariectomized mice, but its effects were significantly blunted in *ATRAID*^{KO} matched cohorts (Fig. 3e-i). Interestingly, the only parameter made worse by alendronate in wild-type mice was post-yield displacement (Fig. 3g). Thus, this measurement, consistent with published literature[56,57], provides a correlate for the downside of taking N-BPs, namely that they might increase bone fragility. Importantly *ATRAID* loss prevented alendronate-mediated reduction in post-yield displacement (Fig. 3g), which suggests that *ATRAID* might contribute to treatment outcome[58].

Because N-BPs potentially affect osteoclasts and osteoblasts, we investigated whether ATRAID deficiency would regulate the effects of alendronate in each cell type in our osteoporosis model. Regarding osteoclasts, in wild-type mice both osteoclast surface per bone surface (Oc.S/BS) and osteoclast number per bone surface (N.Oc/BS) were impaired by alendronate treatment (Fig. 3j, k). In contrast, in *ATRAID*^{KO} mice, alendronate was noticeably less effective on osteoclasts (Fig. 3j, k). That osteoclast number was reduced by N-BPs in wild-type mice is consistent with our cell viability measurements in non-osteoclasts (Fig. 1, 2 and Supplementary Fig. 1, 2) and with previous literature[55].

To provide insight into the effects of N-BPs on osteoblasts in our osteoporosis model, we measured BFR and mineral apposition rate (MAR)[51]. Unlike BFR where the bone formation rate is normalized by the amount of labeled bone surface, MAR is the rate of bone formation irrespective of how much of the bone is active[51]. Alendronate did not affect trabecular MAR or BFR in either wild-type or *ATRAID*^{KO} mice (Fig. 3l, m) suggesting that the osteoblast is not an important determinant of the alendronate-dependent improvements in the bone parameters we measured in our experimental paradigm.

The *ATRAID*-dependent effects we observed of N-BPs on bone are consistent with the osteoclasts and not osteoblasts being a key cell type affected by N-BPs (Fig. 3). As *ATRAID* is expressed well in osteoclast lineage cells (Supplementary Fig. 4)[59], we sought to test whether *ATRAID* functioned cell-autonomously in this cell type. First, we generated *ATRAID* knockout RAW 264.7 cells, a robust, well-characterized murine macrophage cell line (Fig. 4a) that can be differentiated to osteoclast-like cells using RANKL[60]. *ATRAID* deficiency did not impair RAW 264.7 RANKL-induced differentiation (Fig. 4b). This is consistent with our results in mice where basal measures of osteoclast function were not significantly reduced by *ATRAID* deficiency (Supplementary Fig. 3m, n). We treated both RAW 264.7 cells and the RAW 264.7 cells differentiated into osteoclasts with alendronate, and found *ATRAID* deficiency, as expected, conferred resistance to doses that inhibit cell viability (Fig. 4c, d) and induced apoptosis (Fig. 4e). These results are consistent with our effects in the osteoporosis model where alendronate reduced the osteoclast cell number in the bones of wild-type mice, but not in *ATRAID* deficient mice (Fig. 3k). For independent confirmation that *ATRAID* is required cell-autonomously for N-BP-dependent effects in osteoclasts, we isolated M-CSF expanded, bone marrow macrophages (BMMs) from both WT and $ATRAID^{KO}$ mice, and differentiated these cells into osteoclasts following a standard protocol[61]. As with RAW 264.7 cells, $ATRAID^{KO}$ BMMs differentiated into osteoclasts as well as wild-type cells, irrespective of treatment with alendronate (Fig. 4f). Furthermore, BMM-derived $ATRAID^{KO}$ osteoclasts were also resistant to alendronate-induced apoptosis (Fig. 4g). This suggests that *ATRAID* is required cell autonomously in osteoclasts for the effects of N-BPs on cell number.

Alendronate did not affect known markers of osteoclast differentiation in wild-type cells (Fig. 4f). Therefore, to pursue the mechanism of its cell-autonomous effects on osteoclast function, we focused on prenylation. In alendronate-treated RAW 264.7 and differentiated RAW 264.7 to osteoclast cells, we found $ATRAID^{KO}$ cells were resistant to alendronate-induced inhibition of

prenylation (Fig. 4h). In total, these findings suggest that *ATRAID* is required for the cell-autonomous effects of N-BPs on prenylation in its key target cell type – the osteoclast.

The focus of this work has been on *ATRAID* as a novel factor upstream of *FDPS* in a genetic pathway with N-BPs, heretofore the Target of Bisphosphonates (TBONE) pathway (Fig. 4i). This work has focused on prenylation as an output of FDPS function, but recently *FDPS* has been linked to DNA synthesis and damage[40]. Considering that *ATRAID* overexpression induces p53 and senescence[62], it will be interesting to determine whether these effects are mediated by *FDPS*. With statins we identified *WT1*, which is interesting because it is overexpressed in many cancers and downregulates the mevalonate pathway at the level of *FDPS*[63,64]. This suggests that FDPS modulation might be involved in the oncogenic effects of WT1. In addition to SLC37A3, the SLC37A family member[65], *SLC37A2*, is mutated in dogs and gives rise to a bone overgrowth phenotype that resembles the human disease, Caffey syndrome[66,67]. This phenotype is particularly interesting because it suggests that natural ligands for the SLC37A2 transporter might phenocopy N-BP treatment. Lastly, ATRAID binds Nell-1, a secreted protein that promotes bone mineralization in mice and potentiates osteoblast differentiation in an *ATRAID*-dependent manner[68,69]. It is also notable that Nell-1 is in pre-clinical testing for the treatment of osteoporosis[70]. In future studies, it will be interesting to determine whether Nell-1 affects the responses to N-BPs we observe upon manipulating *ATRAID*. There are rare, but serious clinical issues with N-BPs. Therefore, identifying those patients who might experience these consequences when taking N-BPs is of paramount importance. Perhaps utilizing *ATRAID* or other factors characterized herein as biomarker(s) might eventually be such a diagnostic strategy.

Acknowledgements. We thank members of the O'Shea and Peterson laboratories for helpful discussions, especially A. R. Subramaniam, Christopher Chidley, and Anna Puszynska for

illustrations (O'Shea); Chris Chow and Kevin Li (Peterson). We thank Mary Bouxsein and Daniel Brooks (Beth Israel Deaconess Medical Center), and Dan Lieb and Matt Silva (Washington University School of Medicine) for bone structure and function analysis. We thank Kenichi Nagano and Roland Baron (Harvard School of Dental Medicine), Yoshiko Iwamoto (Massachusetts General Hospital) and Deb Novack, Gary London, and Crystal Idleburg for histology, histomorphometry, and imaging (Washington University School of Medicine). We thank Max Haeussler (UCSC) for help with PubMed data mining. This work was supported by grants from the NIH (CA103866 and AI047389 to D.M.S., HD070394 to B.L.) and Department of Defense (W81XWH-07-0448 to D.M.S.); awards from the W.M. Keck Foundation and the LAM (lymphangioleiomyomatosis) Foundation to D.M.S.; Rolanette and Berdon Lawrence Bone Disease Program of Texas and BCM Center for Skeletal Medicine and Biology and NIDDK training grant 5T32DK060445-10 to A.R.; fellowships from the Jane Coffin Childs Foundation, NIH/NIA K99/R00 (1K99AG047255-01/5R00AG047255-04), and NIH/NIAMS P30 AR057235 to T.R.P. D.M.S. and E.K.O are investigators of the Howard Hughes Medical Institute. ATRAID, SNTG1, EPHB1, and PLCL1, the genes identified here, are part of a Whitehead–Harvard patent on which T.R.P., T.R.B., E.K.O., and D.M.S. are inventors. Shared reagents are subject to a materials transfer agreement.

Author Contributions. T.R.P., L.E.S., and E.K.O. designed the study. J.P., A.R., and Z.Y. performed viability assays. S.K. and L.S. performed immunoblots. Y.B., B.H.L, D.T.B. and N.S. conducted analysis of both basal and OVX mouse studies. C.L. performed statistical analysis for the patient gene expression and mouse studies. S.M., J.C.B., M.M., M.S., M.H., S.D., V.N.B., R.C., M.J.G., C.M.M., W.M.R., C.A.G., K.D., M.P.W. performed the exome sequencing on the atypical fracture patients. G.H. and C.C.G. performed statistical analysis for the atypical fracture patients. M.V., K.B., J.E.C., T.R.B., and D.M.S. performed and/or provided assistance with the

haploid screening. J.L. and N.S. performed the CRISPRi screening. T.R.P., J.P., L.E.S. and E.K.O. wrote the paper.

Data availability statement. All data that supports the findings is available in the Figures and Supplementary Figures and Tables.

Figure 1 | *ATRAID* is a genetic factor in the response to nitrogen-containing bisphosphonates in cells and in patients. (a) Schematic of haploid mutagenesis screening pipeline. Sequencing-based identification of gene-trap insertion sites in alendronate-resistant human haploid KBM7 cells. Genomic DNA for sequencing was obtained from mutagenized KBM7 cells grown for four weeks post-treatment with 165 μM alendronate. **(b)** Sequencing-based identification of gene-trap insertion sites in alendronate-resistant cells. N=number of unique insertions within the stated gene locus. False discovery rate corrected (FDR) p-values for *ATRAID*=7.02×10^{-45}, *PLCL1*=1.02×10^{-04}, *EPHB1*=2.05×10^{-04}, *SNTG1*= 1.84×10^{-03}. P-values represent enrichment in alendronate-treated versus vehicle treated cells. The red dotted line indicates the genes with a FDR p-value of < 0.05. 185 genes in this screen that met that criteria. **(c)** Schematic of a molecular biology-optimized, PubMed-based database. Alendronate haploid screen hit genes were queried with terms that identify publications that co-mention the gene name, the indicated tissues of interest, and genome-wide studies. **(d)** PubMed analysis indicates that the alendronate hit genes (false discovery adjusted p-value < 0.05) identified in **(b)** are commonly cited in studies which mention bone and genome-wide studies and they are significantly enriched in the literature compared with 20 randomly chosen, control gene sets. * indicates p = 4.66×10^{-13} using a one sample t-test. **(e)** Schematic of the cholesterol pathway indicating the known mechanistic target for the cholesterol-lowering, statins, HMGCR, and the bone anti-resorptive drugs, N-BPs, FDPS. **(f)** Haploid screening performed as in **(a)** with the statins, lovastatin and simvastatin, yield several novel genes but not *ATRAID*. **(g)** Schematic of CRISPRi mutagenesis screening pipeline. Sequencing-based identification of sgRNAs in drug-

treated human K562 cells. Genomic DNA for sequencing was obtained from mutagenized K562 cells grown for two-three weeks with or without the indicated drugs. **(h)** *ATRAID* and the known N-BP target, *FDPS,* are top ranked hits in a CRISPRi screen with alendronate, but not with several other clinical and experimental drugs. We performed the alendronate CRISPRi screen as part of another work indicated as 'Yu et al'[36]. Rank positions for *ATRAID* and *FDPS* were grouped in the indicated bins and color coded for visual clarity. **(i)** Genome-wide studies of N-BP responsiveness in patients vs. cells and their selected differential gene ontology (GO) categories. The following patient studies used are: osteonecrosis of the jaw (ONJ), breast cancer bone marrow micrometastases (i.e., disseminated tumor cells (DTC)), and atypical femoral fractures (AFF). **(j)** 30 genes including *ATRAID* are statistically significant hits ($p < 0.05$) with zolendronate, differentially expressed in both gene expression datasets (ONJ and DTC), and possess non-synonymous coding variants in AFF cases but not controls. These 30 genes are visualized as the venn diagram of overlap of the following gene lists: significant CRISPRi hits (1787 out of 18903 genes); differentially expressed N-BP in ONJ + DTC (6165 out of 18415 for ONJ; 1854 out of 20492 for DTC; 774 genes are significant when considering both gene sets); coding variant(s) in AFF cases and not controls (2696 out of 13237 genes). **(k)** Patient genetic data for *ATRAID* and *FDPS*. Raw expression values were normalized to 1 to fit on a comparable Y axis. * indicates $p<0.05$. N.S. indicates not significant. "X"-enriched refers to the fold-enrichment of the allele compared with a population with a similar genetic background as the cases. For the AFF sequencing variants, "v3" and "v2" refer to isoforms of the *ATRAID* gene. A simple binomial test was used to calculate the significance of each variant. * indicates $p<0.05$.

Figure 2 | *ATRAID* is required for molecular responses to nitrogen-containing bisphosphonates. (a) Schematic representation of structural features of human ATRAID protein and its mouse and frog orthologues. **(b)** Cell viability in wild-type control and *ATRAID*-

deficient cells exogenously expressing or not expressing *ATRAID* cDNA. Cells were treated with 60 μM alendronate and analyzed for cell viability. Cell viability was determined by measuring cellular ATP levels and is expressed as a ratio of that compared with untreated cells. Error bars indicate the standard deviation for n=4 (biological replicates). N.S., not significant; * indicates $p<0.05$. v2, variant 2 (NM_080592.3); v3, variant 3 (NM_001170795.1) of the *ATRAID* gene, respectively. **(c)** Chemical structures for nitrogen-containing bisphosphonates (N-BPs) or non-nitrogen-containing bisphosphonates (BP) used in **(d)** are shown. **(d)** KBM7 cell viability in *ATRAID*-deficient (ATRAID_GT1 and ATRAID_GT2) and control (wild-type) KBM7 cells upon treatment with nitrogen-containing bisphosphonates (N-BPs) or non-nitrogen-containing bisphosphonates (BP). All cells were treated with the indicated concentration of the indicated N-BP (alendronate, ibandronate, pamidronate, zoledronic acid), BP (etidronate, tiludronate), or **(e)** the statin, lovastatin for 72 hours. Cell viability was determined by measuring cellular ATP levels and is expressed as a ratio of that compared with untreated cells. All measurements were performed in quadruplicate (biological replicates). * indicates $p<0.05$, unpaired *t*-test. **(f)** Alendronate induced inhibition of protein prenylation requires *ATRAID*. *ATRAID*-deficient and *ATRAID* V3-reconstituted HEK-293T cells were treated with the indicated dose of alendronate for 24 hours then lysed and analyzed by immunoblotting for the indicated proteins. Equal amounts of protein were loaded in each lane. This experiment was repeated three times (biological replicates) and was consistent all three times. * indicates non-specific band.

Figure 3 | *ATRAID* is required for organismal responses to nitrogen-containing bisphosphonates. (a) Schematic of menopausal bone loss model – bilateral ovariectomy (OVX). Saline or 100 μg/kg/week alendronate was administered concurrent with OVX or a sham procedure. After four weeks, mice were euthanized and bones and serum were extracted and analyzed. **(b)** Representative μCT reconstructions of femoral trabecular bone from 4-month-old litter-matched derived, wild-type, *ATRAID* WT (+/+), and KO (-/-), female mice that were either

ovariectomized (OVX) or sham operated (Sham), treated with either vehicle (saline) (+OVX), or alendronate (+OVX+ALN) for four weeks. **(c, d)** Ovariectomized *ATRAID*$^{-/-}$ mice have impaired bone microstructural responses to alendronate. Femur trabeculae, **c,** and cortical, **d,** regions were analyzed by μCT. Each circle represents an individual animal. Circles offset to the right represent unique animals with similar values to those of another animal (offset for visual clarity). N=6-11 mice (3.5 month old) per group. * indicates $p<0.01$, $^{\#}$ indicates $0.01<p<0.05$. **(e-g)** Ovariectomized *ATRAID* KO mice have impaired bone strength responses to alendronate. Stiffness, **e**, yield load, **f**, and post-yield displacement, **g,** were analyzed by three-point bending test. Each circle represents an individual animal. Circles offset to the right represent unique animals with similar values to those of another animal (offset for visual clarity). N=6-11 mice per group. *indicates $p<0.01$, $^{\#}$indicates $0.01<p<0.05$. **(h, i)** Ovariectomized *ATRAID* KO mice have impaired serum responses to alendronate. Serum CTX-I, **h,** or total osteocalcin, **I,** were measured by ELISA. N=8-13 mice per group. * indicates $p<0.05$. **(j-m)** Ovariectomized *ATRAID* KO mice have impaired histomorphometric responses to alendronate. Osteoclast surface to bone surface ratio (Oc.S/BS), **j**, and number of osteoclasts per bone surface (N.Oc/BS), **k,** were determined by Tartrate Acid Phosphatase (TRAP)-assay reactivity. Mineral apposition rate (MAR), **l**, and bone formation rate (BFR/BS)**, m,** were determined by double labeling using Calcein followed by Alizarin Red were analyzed histologically. Each circle represents an individual animal. Circles offset to the right represent unique animals with similar values to those of another animal (offset for visual clarity). For **j-m**, N=5-7 mice per group. * indicates $p<0.05$, n.s. indicates not significant.

Figure 4 | ***ATRAID* is required for the effects of alendronate on osteoclasts. (a)** Schematic of the mouse *ATRAID* first coding exon, indicating the CRISPR-induced mutations present in the two *ATRAID*^{KO} clones. **(b)** Quantitative PCR to examine mRNA expression of markers of osteoclast differentiation, *CTSK, RANK, TRAP,* in RAW 264.7 wild-type (WT) and ATRAID^{KO}

cells M-CSF enhanced, bone marrow macrophages (BMMs) differentiated with *RANKL* to osteoclasts. Expression is normalized to wild-type, undifferentiated RAW 264.7 cells, using *ACTB* and *RPLP0* as control genes. Error bars represent the standard deviation of technical triplicate reactions. **(c)** Relative ATP levels, representing cell viability, of RAW 264.7 wild-type (WT) and *ATRAID*^{KO} cell lines that were treated with a two-fold dilution series of alendronate, increasing from 1μM to 640μM, for 48 hours. Relative ATP levels are represented as a ratio of each treated cell line compared with untreated control. Error bars represent the standard deviation of triplicate biological replicates, * indicates $p<0.05$. Scale used on the x-axis is $\log_2$. **(d)** As in **c**, but with RAW-derived osteoclasts, treated with the indicated concentrations of alendronate for 48 hours. **(e)** Percent of Annexin-V positive cells after a 48 hour alendronate treatment in wild-type and *ATRAID*^{KO} differentiated RAW 264.7 osteoclasts. Annexin V staining was assessed using flow cytometry. Error bars represent the standard deviation of n=3 experiments (biological replicates), * indicates $p<0.05$. **(f)** Quantitative PCR for osteoclast markers on mRNA isolated from BMMs derived from *ATRAID* WT (+/+) and KO (-/-) mice differentiated to osteoclasts. Expression is normalized to wild-type, undifferentiated BMMs, using *ACTB* and *RPLP0* as control genes. Error bars represent the standard deviation of triplicate reactions. **(g)** Percent of Annexin-V positive cells after a 48 hour alendronate treatment of differentiated *ATRAID* WT (+/+) and KO (-/-) BMMs into osteoclasts. Annexin V staining was assessed using flow cytometry. Each circle represents osteoclasts derived from an individual animal (split for treatment with 0, 10μM, 30μM alendronate). Red line indicates mean. * indicates $p<0.05$, N.S. indicates not significant. **(h)** Immunoblots of cell lysates of RAW wild-type (WT) and *ATRAID*^{KO} (KO) cells, and RAW 264.7-derived osteoclasts treated with alendronate for 48 hours, demonstrating *ATRAID* deficiency confers resistance to alendronate-induced prenylation defects. Top panel: immunoblot specific to the unprenylated version of Rap1a. Bottom panel: Gapdh, serving as a loading control. Alendronate concentrations were 0, 20μM, 80μM. **(i)** The target of nitrogen-containing, bisphosphonates (TBONE) pathway. Genetic

interactions of ATRAID, FDPS, and N-BPs. (~N) refers to diverse nitrogen-containing, hydrocarbon sidechains.

Materials and Methods

Materials. Reagents were obtained from the following sources: antibodies to Rap1a (SC-1482) from Santa Cruz Biotechnology; anti-HDJ-2/DNAJ Ab-1, Clone: KA2A5.6 ((cat.# MS-225-P0), anti-V5 (cat.# R960-25), and GAPDH (14C10) Rabbit mAb (cat.# 2118S) from Fisher Scientific; rabbit polyclonal and monoclonal antibodies to PARP (cat.# 9532) from Cell Signaling Technology; FuGENE 6 (cat.# E2691) and Complete Protease Cocktail (cat.# 11836170001) from Roche; alendronate (cat.# 1012780-200MG), pamidronate (cat.# P2371-100MG), etidronate (cat.# P5248-10MG), tiludronate (cat.# T4580-50MG), lovastatin (cat.# M2147), simvastatin (cat.# S6196), phenformin (cat.# PHR1573), lithium carbonate (cat.# 62470), fluoxetine (cat.# F132), sertraline (#S6319), Acid Phosphatase Leukocyte (TRAP) kit (cat.# 387A-1KT), SYBR Green JumpStart Taq ReadyMix (cat.# 4309155), calcein (cat.# C0875-5G), FLAG M2 affinity agarose beads (Cat.# M2220), and anti-FLAG antibody (F3165), 3X FLAG peptide (F4799), and alizarin red (cat.# A3882-1G) from Sigma-Aldrich. Zolendronic acid (zolendronate, cat.# M 1875) from Moravek; IMDM Glutatmax, α-MEM, RPMI, SuperScript II Reverse Transcriptase, Platinum Pfx, Platinum Taq DNA Polymerase and inactivated fetal calf serum (IFS) from Invitrogen. MSDC-5514 was a kind gift from Metabolic Solutions Development Company.

Cell lines and cell culture. KBM7 cell lines were cultured in IMDM with 10% IFS. K562 cell lines were cultured in IMDM or RPMI with 10mM Glutamine with 10% FBS. HEK-293T cells were cultured in DMEM with 10% FBS. RAW264.7 and primary mouse cells were cultured as described below.

cDNA manipulations and mutagenesis. The cDNAs for *ATRAID* were cloned from a human R4 cell line cDNA library. For expression studies, all cDNAs were amplified by PCR and the products were subcloned into the Sal 1 and Not 1 sites of pRK5 or pMSCV[71]. The controls, *metap2* and *tubulin*, were previously described[72]. All constructs were verified by DNA sequencing. To generate the 293T *ATRAID_KO* expressing *ATRAID-FLAG*, using Gibson assembly we cloned the cDNA encoding *ATRAID* with a C-terminal Flag tag into a homologous recombination vector targeting the *AAVS1* locus. We transfected this vector along with pX330 expressing an sgRNA targeting the *AAVS1* locus.

sgRNA manipulations. Genome editing experiments were designed based on an established protocol[73]. In brief, the sgRNAs for *ATRAID* were cloned using Golden Gate assembly into pSpCas9-BB-2A-GFP (PX438), a kind gift from Feng Zhang (Addgene #48138). All constructs were verified by PCR and DNA sequencing. For the human *ATRAID* locus, one sgRNA targeting exon 3 and another targeting exon 5 were used to act simultaneously and remove part of exon 3, the entire exon 4 and part of exon 5.

Human *ATRAID*:

exon3 sgRNA_1: GCCTGATGAAAGTTTGGACC

exon3 sgRNA_2: CCCTGGTCCAAACTTTCATC

exon5 sgRNA_1: GTCCTGGAGGAATTAATGCC

exon5 sgRNA_2: GTCCTGGAGGAATTAATGCC

Mouse *ATRAID*:

GGATACATCGAAGCTAATGC

For generating *ATRAID* knockouts in RAW 264.7 cells, cells were transfected with PX438 carrying the above sgRNA. Mutation was confirmed by PCR and sequencing.

Haploid genetic screening. The genetic selection with alendronate, simvastatin, and lovastatin was performed on 100 million mutagenized KBM7 cells[74]. Cells were exposed to 165 μM alendronate, 12 μM simvastatin, or 12 μM lovastatin and allowed to recover for 4 weeks before harvesting the surviving cells and isolating genomic DNA. Analysis of the screen was performed essentially as described previously[74]. In brief, the sequences flanking retroviral insertion sites were determined using inverse PCR followed by Illumina sequencing. After mapping these sequences to the human genome, we counted the number of inactivating mutations (i.e., mutations in the sense orientation or present in exon) per individual Refseq-annotated gene as well as the total number of inactivating insertions for all Refseq-annotated genes. For each gene, statistical enrichment was calculated by comparing how often that gene was mutated in the drug-treated population with how often the gene carries an insertion in the untreated control dataset. For each gene, the P-value (corrected for false discovery rate) was calculated using the one-sided Fisher exact test (Supplementary Table 1).

PubMed citation analysis. We downloaded all PubMed citations via the repository: https://github.com/maximilianh/pubMunch and NCBI aliases from the NCBI website, ftp://ftp.ncbi.nlm.nih.gov/gene/DATA/GENE_INFO/Mammalia/, into separate MySQL database tables. We queried the abstracts for the co-occurrence of the three terms: for 1) <official human NCBI gene symbol>; 2) “GWAS” or “genome-wide” and; 3) <human tissue>. This combination of terms highly enriches for studies involving molecular biology and humans. We also performed natural language processing to exclude abstracts that contain gene symbols, e.g., with common English words such as ACT as well as all “HLA-” containing gene symbols. To determine whether our alendronate haploid screen hit genes that were cited in studies focused on bone significantly more than would occur by chance, we randomly selected 20 control sets of 185 genes and performed a similar analysis to that with our 185 hit genes. The code for this analysis

is available at: https://github.com/tim-peterson/morpheome. The P-value calculation was performed using a one sample t-test using the R function t.test( ). http://stat.ethz.ch/R-manual/R-devel/library/stats/html/t.test.html.

CRISPRi genetic screening. Version 2 of the CRISPRi library was used and screens were performed as previously described[75]. The goal of these screens is to determine the extent to which a gene knockdown affects cell growth in the presence of the selection pressure, i.e., drug, (after normalizing by growth in the absence of drug). We used all drugs at a half-maximal inhibitory concentration (IC50) value[76] – a common measure of drug potency. After drug selection, high-throughput sequencing of DNA from treated and untreated cells was performed to identify genes which when inactivated alter cell growth rate most significantly. Two biological replicates were used for each of the three conditions: T0, untreated, and treated. The sequencing analysis pipeline source code is available here: https://github.com/mhorlbeck/ScreenProcessing. Statistical significance is based on the concept of the false discovery rate[77]. We employed formulas for deriving cellular phenotypes from cell fraction measurements in a population at discrete time-points[78].

For comparison of the ranking of *ATRAID* and *FDPS* in the alendronate screen vs. the screens with the indicated other drugs gene rank position for all ~37,810 sgRNA gene sets (gene targeting and negative control) was determined by taking the absolute value of their ρ (rho) values for the average of their top three sgRNAs.

Transcriptional profiling analysis. The multiple myeloma, osteonecrosis of the jaw (ONJ) microarray gene expression was performed using Affymetrix U133 Plus 2.0 array platform (Affymetrix, Santa Clara, CA, USA) as previously described[41]. 21 multiple myeloma patients with a history of N-BP use were included in the study. 11 patients (52.4%) reported to have ONJ.

The breast cancer bone marrow micrometastases microarray gene expression data also used the Affymetrix U133 Plus 2.0 array platform. 54 breast cancer patients treated with zometa (zolendronate) were included in the study. 14 patients (25.9%) eventually died and 40 patients (74.1%) survived. Her-2 negative patients were divided into two categories following randomization to the zolendronate arm: those that who had DTC reoccurrences or lived less than 1000 days and those who lived at least 2500 days.

Quantile normalization was used for all differential expression analysis, and all the normalization procedures were performed using function normalizeQuantiles in the R Bioconductor package limma[79]. Gene expression data was filtered using function filterfun in the R Bioconductor package genefilter[80]. Probes with expression values over 5 in less than 25% of the samples were removed. Comparison between groups were estimated using an empirical Bayes method[81], and variances across all genes were used to estimate the variance of each gene. Raw p-values were calculated from a moderate t-test, and false discovery rate (FDR) adjusted p-values were obtained based on Benjamini and Hochberg's methods for multiple testing. Log_2 fold changes between the experimental conditions were calculated for each gene as well.

Affy probe IDs were transformed into gene symbols based on the R Bioconductor package, hgu133plus2.db[82]. In Fig. 1i, j, differentially regulated genes for the -/+ONJ patients were identified by having adjusted p-values smaller than 0.05, while potential differentially-regulated genes for the <1000 vs. >2500 days with breast cancer patients with disseminated tumor cells (DTC) were identified by having raw p-value smaller than 0.05. For the ONJ dataset, 2383 genes were significant. For the DTC dataset 2174 genes were significant.

Exome sequencing analysis. Exome sequencing data was generated for 27 bisphosphonate treated osteoporosis cases with atypical femoral fractures (AFF) and 11 bisphosphonate treated

osteoporosis cases without atypical femoral fractures. Exome capture was performed using Agilent All-exome capture kits. Sequencing was performed using paired-end Illumina sequencing. Alignment was performed using the Burrows-Wheeler Aligner (BWA) and variants called using SAMTOOLS. Variant positions were processed excluding those with call rates <0.95 or Hardy-Weinberg equilibrium P-values < 10^{-5}. Genotypes were filtered excluding those with read depth <8x or genotype quality (GQ) < 20. From dbSNP, https://www.ncbi.nlm.nih.gov/SNP/ : For the *ATRAID* gene, the D5G variant is found on chromosome 2 position: 27212382 - rs1275533. For the G32R variant is found on chromosome 2 position: 27212297 - rs11556163. For the *FDPS* gene, the P16L variant is found on chromosome 1 position: 155309836 - rs142276507. For the *FDPS* V364A variant is found on chromosome 1 position: 155320440 - rs41314549.

The ethnic breakdown of the AFF cases is: 25/28 European American (EA), 3/28 Asian American (AA), 0/28 African American. The ethnic breakdown of the controls is 8/11 European American and 3/11 unknown. For *ATRAID*, the D5G variant is present in 2 out of 28 AFF patients. Though this allele wasn't detected in the 11 control samples, it is present in a population of European Americans (EA) that is representative of the study population at a prevalence of 0.0139 and in Asian Americans (AA) at a prevalence of 0.002. Therefore, the D5G allele is (2/28) / (0.0139 * 25/28 + 0.002 * 3/28) = 5.66X enriched in cases compared to a representative population to that of the cases. A simple binomial test, binom.test(), was used to calculate the p-value for each variant. For the D5G allele, p-value = 0.04851. For the G32R *ATRAID* allele the enrichment is: (2/28) / (0.0149 * 25/28 + 0.002 * 3/28) = 5.28; p-value = 0.05477. For *FDPS*, the P16L the enrichment is: (1/28) / (0.00014043) = 254.32; p-value = 0.003925. The ethnic breakdown for this variant is unknown. For the V364A *FDPS* allele, the enrichment is (2/28) / (0.0318 * 25/28 + 0.0102 * 3/28) = 2.42X; p-value = 0.1995.

Cell viability assays. Wild-type or mutant cells were seeded at 20,000 cells per well in a 96-well tissue culture plate and treated with indicated concentrations of compound or left untreated. 48 or 72 hours after treatment the cell viability was measured using a Cell-titer Glo colorimetric assay (Promega) according to manufacturer's protocol. Viability is plotted as percentage viability compared to untreated control.

For assays of apoptosis, cells were plated in 6-well dishes and exposed to alendronate for 48 hours. AnnexinV positive cells were quantified using flow cytometry with the Dead Cell Apoptosis Kit with AnnexinV Alexa Fluor (488) and PI (Thermo Fisher Scientific #V13241) following the manufacturer's instructions.

Protein analysis. All cells unless otherwise stated were rinsed twice with ice-cold PBS and lysed with Triton-X 100 or NP-40 containing lysis buffer (40 mM HEPES [pH 7.4], 2 mM EDTA, 150 mM NaCl, 50 mM NaF, 1% Triton-X 100 or 1% NP-40, and one tablet of EDTA-free protease inhibitors [Roche] per 25 ml or Halt protease-phosphatase inhibitor (#78442 ThermoFisher Scientific)). Lysate is incubated at 4 centigrade for 15-30min with constant inversion. The soluble fractions of cell lysates were isolated by centrifugation at 13,000 rpm for 10 min in a microcentrifuge. Lysate protein concentrations were normalized by Bradford assay (Bio-Rad). Proteins were then denatured by the addition of sample buffer and by boiling for 5 minutes, resolved using 4%-20% or 6% (for HDJ-2) SDS-PAGE (Invitrogen), and analyzed by immunoblotting for the indicated proteins. Immunoblotting was performed as follows: nitrocellulose membranes were blocked at room temperature (RT) with 5% non-fat milk for 45min. Membranes were then incubated overnight at 4^{o}C with desired primary antibodies dissolved in 5% milk. Membranes were then washed 3 times in TBST, each wash lasting 5min.

Membranes were then incubated at RT with desired secondary antibodies at 1:2000 in 5% milk for 45min. HRP-conjugated or fluorescent secondary antibodies (Santa Cruz Biotechnology or Thermo Fisher, respectively) were used for detection. Membranes were then washed 3 times in TBST, each wash lasting 5min. Signal from membranes using HRP-conjugated secondary antibodies were captured using a camera and those using fluorescent secondary antibodies were imaged on a GE Typhoon Trio imager. The small GTPase Rap1A protein prenylation can be detected by Western blot analysis using an antibody that specifically binds to its unprenylated form[83,84] (Santa Cruz, SC-1482).

RAW 264.7 differentiation. RAW 264.7 cells were maintained in DMEM + 10% FBS + 1X penicillin/streptomycin. Differentiation of RAW cells to osteoclasts was achieved following the protocol of Collin-Osdoby et al.[60] where cells were treated with 35ng/ml RANKL (R&D Systems) for 6 days. For experiments with alendronate, the drug was added at the indicated concentrations 48 hours prior to collection.

Primary bone marrow isolation and osteoclast differentiation. Primary bone marrow was isolated from the femurs, tibiae, and spine of wildtype and *ATRAID*^{KO} mice, enriched to macrophages and differentiated to osteoclasts following the protocol of Tevlin et al.[61]. Where indicated, cells were treated with the indicated concentration of alendronate 48 hours before collection.

Gene expression analysis. Total RNA was isolated and reverse-transcription was performed from cells or tissues in the indicated conditions. The resulting cDNA was diluted in DNase-free water (1:20) followed by quantification by real-time PCR. mRNA transcript levels were measured using Applied Biosystems 7900HT Sequence Detection System v2.3 software. All Data are

expressed as the ratio between the expression of target gene to the housekeeping genes 36B4 and/or GAPDH. Each treated sample was normalized to the level of the controls in the same cell type.

Human Primer sequences (for clarity, denoted with prefix: “h” for human):

hATRAID exon1-F’ – GGATGGAGGGGCCCGAGTTTCTG

hATRAID exon2-R’ – CCCAAGATGGTGCCCTTCTGATTC

hATRAID exon6-F’ – CCATGGATACAAGTGTATGCGCC

hATRAID exon 7-R’ – TCATGAAGTCTTGGCTTTTCGGC

Mouse Primer sequences (for clarity, denoted with prefix: “m” for mouse):

mATRAID exon3-F’ – GATCTTCAGAACTGTTCCCTGAAG

mATRAID exon4-R’ – GCTGAGTAAACCCACGGAAGGTG

mATRAID exon5-F’ – CTTCTTTCAAGGACAAGCAGATTTG

mATRAID exon 7-R’ – GAATCCCAAAGAACATAAGCAGTG

mACTB- F’- TGTCGAGTCGCGTCCA

mACTB- R’ – ATGCCGGAGCCGTTGTC

mRPLP0- F’ – TGCTCGACATCACAGAGCAG

mRPLP0- R’ – ACGCGCTTGTACCCATTGAT

mCTSK – F’ – CCTTCCAATACGTGCAGCAG

mCTSK- R’ – CATTTAGCTGCCTTTGCCGT

mRANK – F' – GCAGCTCAACAAGGATACGG

mRANK – R'- TAGCTTTCCAAGGAGGGTGC

mTRAP –F' – AAGAGATCGCCAGAACCGTG

mTRAP – R' - CGTCCTCAAAGGTCTCCTGG

Generation and genotyping of ATRAID* KO *mice. Chimeric mice were obtained by microinjection of the correctly targeted *ATRAID* EUCOMM ES clones (HEPD0577_2_D01 and HEPD0577_2_E01)[85,86] into BALB/C blastocysts and crossed with C57BL/6 mice to obtain offspring with germline transmission. Heterozygous mice for the floxed *ATRAID* allele (*ATRAID*$^{loxP/+}$), were crossed to C57BL/6 mice expressing the Cre-recombinase transgene from the full-body CMV promoter[87]. Mice analyzed in this study were 100% C57BL/6.

All experiments involving mice were performed with protocols approved by the Harvard and Washington University Animal Studies Committees. We confirm that we have complied with all relevant ethical regulations. All mice were housed under a 12-hour light cycle and fed standard chow diet ad libitum.

PCR genotyping of all WT and *ATRAID* deficient mice were performed with primers that detect the following:

1) This generates a 140bp product and indicates the presence of the transgene.

Transgene (92 upstream) F' CAGCCATATCACATCTGTAGAG

Transgene (92 upstream) R' GAGTTTGGACAAACCACAACTAG

2) This indicates recombination and is detectable in mice also expressing CRE

Del F' CTGCATTCTAGTTGTGGTTTGTCC

Del R' CAGGAGGTAGTGCAAGCCTTTG

3) Wild-type *ATRAID* primers spanning *ATRAID* exons 3 and 4. This PCR product is not detectable in homozygous null animals.

Exon 3/4 F' CAGAACTGTTCCCTGAAGGATCCTGGTC

Exon 3/4 R' GTACACACTGTTAGCGCTCTGTTTGC

4) These generic CRE primers give a ~100bp product indicates the presence of the CRE transgene.

CRE F' GCG GTC TGG CAG TAA AAA CTA TC

CRE R' GTG AAA CAG CAT TGC TGT CAC TT

Serum ELISA assays. Cardiac puncture blood of mice of the indicated ages was obtained and centrifuged at low speed at 4°C for 15 min, and serum was isolated. Gla-Osteocalcin (Mouse Gla-Osteocalcin High Sensitive EIA Kit from Clontech, cat.# MK127), C-terminus cross-linked telopeptides of type I collagen CTX-I (RatLaps EIA Kit from Immunodiagnosticsystems Inc., Bolden, UK, AC-06F1), and total Osteocalcin (Mouse Osteocalcin EIA Kit from Biomedical Technologies Inc., Stoughton, MA) were quantified following the manufacturer instructions.

Animal procedures. Age and sex matched mice were randomly assigned to treatment groups within each genotype. All animal experiments were replicated two to four times spanning independent days to ensure reproducibility.

Ovariectomy or sham operations were performed on 3.5-month-old females as detailed previously[88]. Briefly, the ovaries were exposed through an abdominal approach and either resected after clipping the blood vessels or left in place (sham operation). The muscle and skin of the abdomen were sutured. Mice were given an intraperitoneal injection of buprenex immediately after surgery and then every twelve hours for 48 hours post-surgery. Immediately

preceding OVX, vehicle (phosphate buffered saline) or 100 µg/kg alendronate (both provided by Sigma) was injected intra-peritoneally every week for 4 weeks. These doses were chosen based on the anti-resorptive activity of alendronate in different species[89,90].

Bone microstructure. A high-resolution desktop micro-tomographic imaging system (µCT40, Scanco Medical AG, Bruttisellen, Switzerland) was used to assess cortical and trabecular bone microarchitecture and morphology in the femoral mid-diaphysis and distal metaphysis, respectively. Scans were acquired using a 10 μm^3 isotropic voxel size, 70 kVP peak x-ray tube potential, 114 mAs x-ray intensity, 200 ms integration time, and were subjected to Gaussian filtration and segmentation. Regions of interest (ROIs) were selected 50 slices above and below the femoral longitudinal midpoint or 100 slices above the growth plate of the distal femur to evaluate the cortical and trabecular compartment, respectively. Image acquisition and analysis adhered to the JBMR guidelines for the use of µCT for the assessment of bone microarchitecture in rodents[48].

Bone biomechanics. Mechanical testing in a 3-point bending to failure was conducted on femora after µCT. Briefly, hydrated femora were stabilized over supports 7mm apart and a loading force was applied in the anteroposterior direction midway between the supports (Instron, Norwood, MA, USA). Test curves were analyzed to determine ultimate force to failure and stiffness as described previously[49,91].

Bone histomorphometry. To label mineralizing fronts, mice were injected intraperitoneally with calcein (15 mg/kg i.p., Sigma-Aldrich) and alizarin red (30 mg/kg; Sigma) were intraperitoneally injected 7 and 2 days, respectively, before euthanasia. Bone was fixed in 10%(vol/vol) neutral buffered formalin for 24 h, processed through a series of graded alcohols, and decalcified. Decalcified vertebrae or femurs were embedded in paraffin and 2-4 h, processed through a

series of graded alcohols, and Tartrate resistant acid phosphatase (TRAP) stain was performed. Undecalcified femora were embedded in methyl methacrylate and the whole bone were cut and stained for TRAP or analyzed for calcein and alizarin red fluorescence. Quantitative histomorphometry was performed using a commercial software (OSTEO II, Bioquant, Nashville, TN, USA), and standard parameters of bone remodeling were determined as detailed elsewhere[92].

Statistics analysis. Unless otherwise specified, group means were compared by one-tailed Student t-test for unpaired samples. Data on repeated measures were analyzed by ANOVA, followed by a post-hoc multiple Holm–Sidak method t-test. All data are expressed as the mean ± s.d with numbers of samples indicated in figure legends. *P* values are indicated in each figure legend, and values less than 0.05 were considered significant.

References:

1. Carey, J.J. & Palomo, L. Bisphosphonates and osteonecrosis of the jaw: innocent association or significant risk? *Cleveland Clinic journal of medicine* **75**, 871-879 (2008).
2. van den Bergh, J.P., van Geel, T.A. & Geusens, P.P. Osteoporosis, frailty and fracture: implications for case finding and therapy. *Nat Rev Rheumatol* **8**, 163-172 (2012).
3. Coleman, R.E. & McCloskey, E.V. Bisphosphonates in oncology. *Bone* **49**, 71-76 (2011).
4. Black, D.M. & Rosen, C.J. Clinical Practice. Postmenopausal Osteoporosis. *N Engl J Med* **374**, 254-262 (2016).
5. Watts, N.B. & Diab, D.L. Long-term use of bisphosphonates in osteoporosis. *J Clin Endocrinol Metab* **95**, 1555-1565 (2010).
6. Bi, Y.*, et al.* Bisphosphonates cause osteonecrosis of the jaw-like disease in mice. *Am J Pathol* **177**, 280-290 (2010).
7. Khosla, S.*, et al.* Addressing the Crisis in the Treatment of Osteoporosis: A Path Forward. *J Bone Miner Res* (2016).
8. Luckman, S.P.*, et al.* Nitrogen-containing bisphosphonates inhibit the mevalonate pathway and prevent post-translational prenylation of GTP-binding proteins, including Ras. *J Bone Miner Res* **13**, 581-589 (1998).
9. van Beek, E., Pieterman, E., Cohen, L., Lowik, C. & Papapoulos, S. Nitrogen-containing bisphosphonates inhibit isopentenyl pyrophosphate isomerase/farnesyl pyrophosphate synthase activity with relative potencies corresponding to their antiresorptive potencies in vitro and in vivo. *Biochem Biophys Res Commun* **255**, 491-494 (1999).

10. Bergstrom, J.D., Bostedor, R.G., Masarachia, P.J., Reszka, A.A. & Rodan, G. Alendronate is a specific, nanomolar inhibitor of farnesyl diphosphate synthase. *Arch Biochem Biophys* **373**, 231-241 (2000).
11. Favus, M.J. Bisphosphonates for osteoporosis. *N Engl J Med* **363**, 2027-2035 (2010).
12. Rosen, C.J. Clinical practice. Postmenopausal osteoporosis. *N Engl J Med* **353**, 595-603 (2005).
13. Coleman, R. The use of bisphosphonates in cancer treatment. *Ann N Y Acad Sci* **1218**, 3-14 (2011).
14. Jha, S., Wang, Z., Laucis, N. & Bhattacharyya, T. Trends in Media Reports, Oral Bisphosphonate Prescriptions, and Hip Fractures 1996-2012: An Ecological Analysis. *J Bone Miner Res* **30**, 2179-2187 (2015).
15. Reszka, A.A. & Rodan, G.A. Nitrogen-containing bisphosphonate mechanism of action. *Mini Rev Med Chem* **4**, 711-719 (2004).
16. Breuil, V.*, et al.* Human osteoclast formation and activity in vitro: effects of alendronate. *J Bone Miner Res* **13**, 1721-1729 (1998).
17. Zimolo, Z., Wesolowski, G. & Rodan, G.A. Acid extrusion is induced by osteoclast attachment to bone. Inhibition by alendronate and calcitonin. *J Clin Invest* **96**, 2277-2283 (1995).
18. Hughes, D.E.*, et al.* Bisphosphonates promote apoptosis in murine osteoclasts in vitro and in vivo. *J Bone Miner Res* **10**, 1478-1487 (1995).
19. Romanello, M.*, et al.* Bisphosphonates activate nucleotide receptors signaling and induce the expression of Hsp90 in osteoblast-like cell lines. *Bone* **39**, 739-753 (2006).
20. Duque, G. & Rivas, D. Alendronate has an anabolic effect on bone through the differentiation of mesenchymal stem cells. *J Bone Miner Res* **22**, 1603-1611 (2007).
21. Karsenty, G. Transcriptional control of skeletogenesis. *Annu Rev Genomics Hum Genet* **9**, 183-196 (2008).
22. Plotkin, L.I.*, et al.* Prevention of osteocyte and osteoblast apoptosis by bisphosphonates and calcitonin. *J Clin Invest* **104**, 1363-1374 (1999).
23. Garcia-Moreno, C.*, et al.* Effect of alendronate on cultured normal human osteoblasts. *Bone* **22**, 233-239 (1998).
24. Baron, R., Ferrari, S. & Russell, R.G. Denosumab and bisphosphonates: different mechanisms of action and effects. *Bone* **48**, 677-692 (2011).
25. Carette, J.E.*, et al.* Haploid genetic screens in human cells identify host factors used by pathogens. *Science* **326**, 1231-1235 (2009).
26. Roelofs, A.J., Thompson, K., Ebetino, F.H., Rogers, M.J. & Coxon, F.P. Bisphosphonates: molecular mechanisms of action and effects on bone cells, monocytes and macrophages. *Curr Pharm Des* **16**, 2950-2960 (2010).
27. Zhu, F.*, et al.* Improved PCR-based subtractive hybridization strategy for cloning differentially expressed genes. *Biotechniques* **29**, 310-313 (2000).
28. Bashiardes, S.*, et al.* SNTG1, the gene encoding gamma1-syntrophin: a candidate gene for idiopathic scoliosis. *Hum Genet* **115**, 81-89 (2004).
29. Liu, Y.Z.*, et al.* Identification of PLCL1 gene for hip bone size variation in females in a genome-wide association study. *PLoS One* **3**, e3160 (2008).
30. Shimizu, E., Tamasi, J. & Partridge, N.C. Alendronate affects osteoblast functions by crosstalk through EphrinB1-EphB. *J Dent Res* **91**, 268-274 (2012).
31. Oesterle, A., Laufs, U. & Liao, J.K. Pleiotropic Effects of Statins on the Cardiovascular System. *Circ Res* **120**, 229-243 (2017).
32. Wang, T.*, et al.* Identification and characterization of essential genes in the human genome. *Science* **350**, 1096-1101 (2015).
33. Hart, T.*, et al.* High-Resolution CRISPR Screens Reveal Fitness Genes and Genotype-Specific Cancer Liabilities. *Cell* **163**, 1515-1526 (2015).

34. Blomen, V.A.*, et al.* Gene essentiality and synthetic lethality in haploid human cells. *Science* **350**, 1092-1096 (2015).
35. Gilbert, L.A.*, et al.* Genome-Scale CRISPR-Mediated Control of Gene Repression and Activation. *Cell* **159**, 647-661 (2014).
36. Yu, Z.*, et al.* Identification of a transporter complex responsible for the cytosolic entry of nitrogen-containing-bisphosphonates. *Elife* **7**(2018).
37. Li, Y.*, et al.* AMPK phosphorylates and inhibits SREBP activity to attenuate hepatic steatosis and atherosclerosis in diet-induced insulin-resistant mice. *Cell Metab* **13**, 376-388 (2011).
38. Raeder, M.B., Ferno, J., Glambek, M., Stansberg, C. & Steen, V.M. Antidepressant drugs activate SREBP and up-regulate cholesterol and fatty acid biosynthesis in human glial cells. *Neurosci Lett* **395**, 185-190 (2006).
39. Park, J.W., Li, J., Kumar, S., Burrow, D., Song, N., Chow, C., Peterson, T.R. MORPHEOME: a resource to identify the molecular functions for orphan genes. *in preparation* (2018).
40. Horlbeck, M.A., Xu, A., Wang, M., Bennett, N.K., Park, C.Y., Bogdanoff, D., Adamson, B., Chow, E.D., Kampmann, M., Peterson, T.R., Nakamura, K., Fischbach, M.A., Weissman, J.S., Gilbert, L.A. Mapping the genetic landscape of human cells. (under review).
41. Raje, N.*, et al.* Clinical, radiographic, and biochemical characterization of multiple myeloma patients with osteonecrosis of the jaw. *Clin Cancer Res* **14**, 2387-2395 (2008).
42. Xiang, J.*, et al.* CXCR4 Protein Epitope Mimetic Antagonist POL5551 Disrupts Metastasis and Enhances Chemotherapy Effect in Triple-Negative Breast Cancer. *Mol Cancer Ther* **14**, 2473-2485 (2015).
43. Yang, G.*, et al.* Identification of the distinct promoters for the two transcripts of apoptosis related protein 3 and their transcriptional regulation by NFAT and NFkappaB. *Mol Cell Biochem* **302**, 187-194 (2007).
44. Phyre2. http://www.sbg.bio.ic.ac.uk/phyre2/html/page.cgi?id=index. *Protein Homology/analogY Recognition Engine V 2.0* (website).
45. Russell, R.G. Bisphosphonates: the first 40 years. *Bone* **49**, 2-19 (2011).
46. Thompson, K., Rogers, M.J., Coxon, F.P. & Crockett, J.C. Cytosolic entry of bisphosphonate drugs requires acidification of vesicles after fluid-phase endocytosis. *Mol Pharmacol* **69**, 1624-1632 (2006).
47. Skarnes, W.C.*, et al.* A conditional knockout resource for the genome-wide study of mouse gene function. *Nature* **474**, 337-342 (2011).
48. Bouxsein, M.L.*, et al.* Guidelines for assessment of bone microstructure in rodents using micro-computed tomography. *J Bone Miner Res* **25**, 1468-1486 (2010).
49. http://www.musculoskeletalcore.wustl.edu/mm/files/Understanding 3pt Bending outcomes.pdf.
50. Rosenquist, C.*, et al.* Serum CrossLaps One Step ELISA. First application of monoclonal antibodies for measurement in serum of bone-related degradation products from C-terminal telopeptides of type I collagen. *Clin Chem* **44**, 2281-2289 (1998).
51. Dempster, D.W.*, et al.* Standardized nomenclature, symbols, and units for bone histomorphometry: a 2012 update of the report of the ASBMR Histomorphometry Nomenclature Committee. *J Bone Miner Res* **28**, 2-17 (2013).
52. Ballanti, P.*, et al.* Tartrate-resistant acid phosphate activity as osteoclastic marker: sensitivity of cytochemical assessment and serum assay in comparison with standardized osteoclast histomorphometry. *Osteoporos Int* **7**, 39-43 (1997).
53. Ferron, M.*, et al.* Insulin signaling in osteoblasts integrates bone remodeling and energy metabolism. *Cell* **142**, 296-308 (2010).

54. Fleisch, H.A. Bisphosphonates: preclinical aspects and use in osteoporosis. *Ann Med* **29**, 55-62 (1997).
55. Watkins, M.P.*, et al.* Bisphosphonates improve trabecular bone mass and normalize cortical thickness in ovariectomized, osteoblast connexin43 deficient mice. *Bone* **51**, 787-794 (2012).
56. Allen, M.R., Reinwald, S. & Burr, D.B. Alendronate reduces bone toughness of ribs without significantly increasing microdamage accumulation in dogs following 3 years of daily treatment. *Calcif Tissue Int* **82**, 354-360 (2008).
57. Lloyd, A.A.*, et al.* Atypical fracture with long-term bisphosphonate therapy is associated with altered cortical composition and reduced fracture resistance. *Proc Natl Acad Sci U S A* (2017).
58. Kennel, K.A. & Drake, M.T. Adverse effects of bisphosphonates: implications for osteoporosis management. *Mayo Clin Proc* **84**, 632-637; quiz 638 (2009).
59. BioGPS. http://biogps.gnf.org/ - goto=welcome. (2011).
60. Collin-Osdoby, P. & Osdoby, P. RANKL-mediated osteoclast formation from murine RAW 264.7 cells. *Methods Mol Biol* **816**, 187-202 (2012).
61. Tevlin, R.*, et al.* Osteoclast derivation from mouse bone marrow. *J Vis Exp*, e52056 (2014).
62. Han, S., Lu, Q. & Wang, N. Apr3 accelerates the senescence of human retinal pigment epithelial cells. *Mol Med Rep* **13**, 3121-3126 (2016).
63. Rae, F.K.*, et al.* Anlaysis of complementary expression profiles following WT1 induction versus repression reveals the cholesterol/fatty acid synthetic pathways as a possible major target of WT1. *Oncogene* **23**, 3067-3079 (2004).
64. Hastie, N.D. Wilms' tumour 1 (WT1) in development, homeostasis and disease. *Development* **144**, 2862-2872 (2017).
65. Chou, J.Y. & Mansfield, B.C. The SLC37 family of sugar-phosphate/phosphate exchangers. *Curr Top Membr* **73**, 357-382 (2014).
66. Hytonen, M.K.*, et al.* Molecular Characterization of Three Canine Models of Human Rare Bone Diseases: Caffey, van den Ende-Gupta, and Raine Syndromes. *PLoS Genet* **12**, e1006037 (2016).
67. Guerin, A., Dupuis, L. & Mendoza-Londono, R. Caffey Disease. in *GeneReviews((R))* (eds. Adam, M.P.*, et al.*) (Seattle (WA), 1993).
68. Zou, X.*, et al.* NELL-1 binds to APR3 affecting human osteoblast proliferation and differentiation. *FEBS Lett* **585**, 2410-2418 (2011).
69. Desai, J.*, et al.* Nell1-deficient mice have reduced expression of extracellular matrix proteins causing cranial and vertebral defects. *Hum Mol Genet* **15**, 1329-1341 (2006).
70. James, A.W.*, et al.* NELL-1 in the treatment of osteoporotic bone loss. *Nat Commun* **6**, 7362 (2015).
71. Peterson, T.R.*, et al.* mTOR complex 1 regulates lipin 1 localization to control the SREBP pathway. *Cell* **146**, 408-420 (2011).
72. Peterson, T.R.*, et al.* DEPTOR is an mTOR inhibitor frequently overexpressed in multiple myeloma cells and required for their survival. *Cell* **137**, 873-886 (2009).
73. Ran, F.A.*, et al.* Genome engineering using the CRISPR-Cas9 system. *Nat Protoc* **8**, 2281-2308 (2013).
74. Carette, J.E.*, et al.* Global gene disruption in human cells to assign genes to phenotypes by deep sequencing. *Nat Biotechnol* **29**, 542-546 (2011).
75. Horlbeck, M.A.*, et al.* Compact and highly active next-generation libraries for CRISPR-mediated gene repression and activation. *Elife* **5**(2016).
76. https://en.wikipedia.org/wiki/IC50.
77. Storey, J.D. & Tibshirani, R. Statistical significance for genomewide studies. *Proc Natl Acad Sci U S A* **100**, 9440-9445 (2003).

78. Bassik, M.C.*, et al.* A systematic mammalian genetic interaction map reveals pathways underlying ricin susceptibility. *Cell* **152**, 909-922 (2013).
79. Bolstad, B.M., Irizarry, R.A., Astrand, M. & Speed, T.P. A comparison of normalization methods for high density oligonucleotide array data based on variance and bias. *Bioinformatics* **19**, 185-193 (2003).
80. Gentleman R, C.V., Huber W and Hahne F genefilter: methods for filtering genes from high-throughput experiments. R package version 1.58.1. (2017).
81. Smyth, G.K. Linear models and empirical bayes methods for assessing differential expression in microarray experiments. *Stat Appl Genet Mol Biol* **3**, Article3 (2004).
82. Carlson, M. hgu133plus2.db: Affymetrix Human Genome U133 Plus 2.0 Array annotation data (chip hgu133plus2). . (2016).
83. Coxon, F.P.*, et al.* Protein geranylgeranylation is required for osteoclast formation, function, and survival: inhibition by bisphosphonates and GGTI-298. *J Bone Miner Res* **15**, 1467-1476 (2000).
84. Frith, J.C., Monkkonen, J., Auriola, S., Monkkonen, H. & Rogers, M.J. The molecular mechanism of action of the antiresorptive and antiinflammatory drug clodronate: evidence for the formation in vivo of a metabolite that inhibits bone resorption and causes osteoclast and macrophage apoptosis. *Arthritis and rheumatism* **44**, 2201-2210 (2001).
85. Kuhn, R. & Torres, R.M. Cre/loxP recombination system and gene targeting. *Methods Mol Biol* **180**, 175-204 (2002).
86. http://www.mousephenotype.org/data/alleles/MGI:1918918/tm1a%2528EUCOMM%2529Hmgu?
87. Schwenk, F., Baron, U. & Rajewsky, K. A cre-transgenic mouse strain for the ubiquitous deletion of loxP-flanked gene segments including deletion in germ cells. *Nucleic Acids Res* **23**, 5080-5081 (1995).
88. Lai, C.F.*, et al.* Accentuated ovariectomy-induced bone loss and altered osteogenesis in heterozygous N-cadherin null mice. *J Bone Miner Res* **21**, 1897-1906 (2006).
89. Fuchs, R.K., Phipps, R.J. & Burr, D.B. Recovery of trabecular and cortical bone turnover after discontinuation of risedronate and alendronate therapy in ovariectomized rats. *J Bone Miner Res* **23**, 1689-1697 (2008).
90. Allen, M.R., Iwata, K., Phipps, R. & Burr, D.B. Alterations in canine vertebral bone turnover, microdamage accumulation, and biomechanical properties following 1-year treatment with clinical treatment doses of risedronate or alendronate. *Bone* **39**, 872-879 (2006).
91. Willinghamm, M.D.*, et al.* Age-related changes in bone structure and strength in female and male BALB/c mice. *Calcif Tissue Int* **86**, 470-483 (2010).
92. Grimston, S.K.*, et al.* Connexin43 deficiency reduces the sensitivity of cortical bone to the effects of muscle paralysis. *J Bone Miner Res* **26**, 2151-2160 (2011).

Figure 1

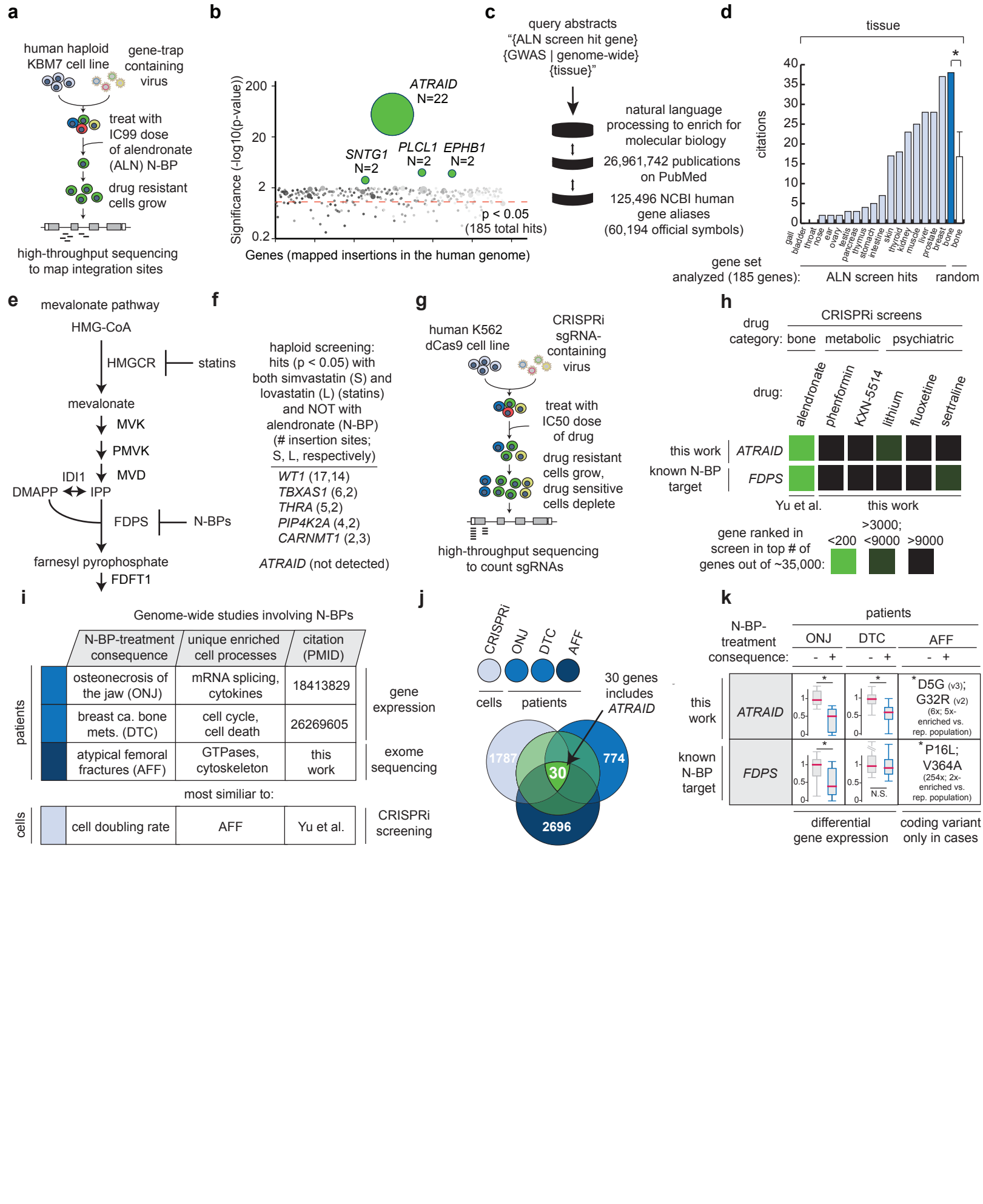

Figure 2

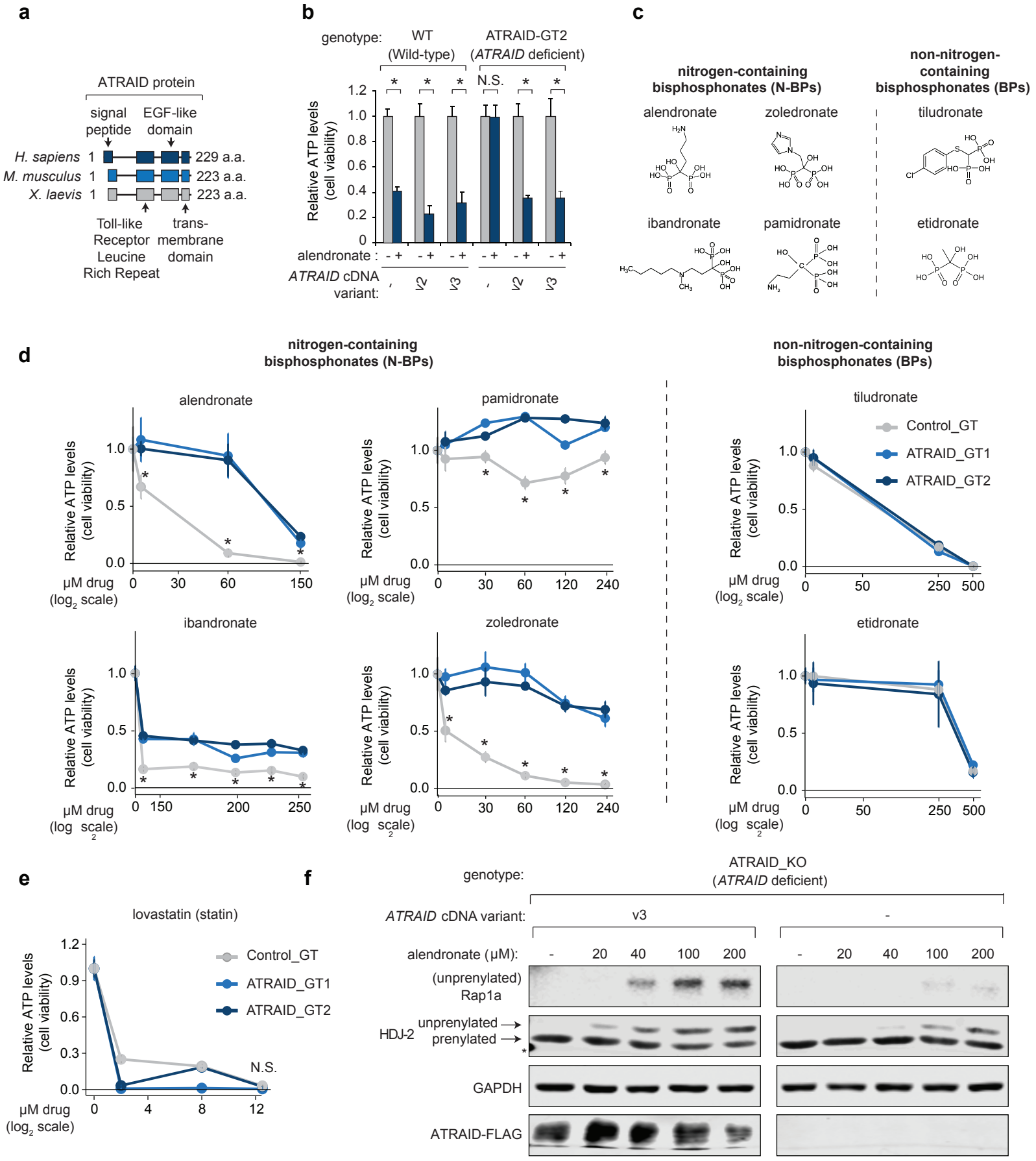

Figure 3

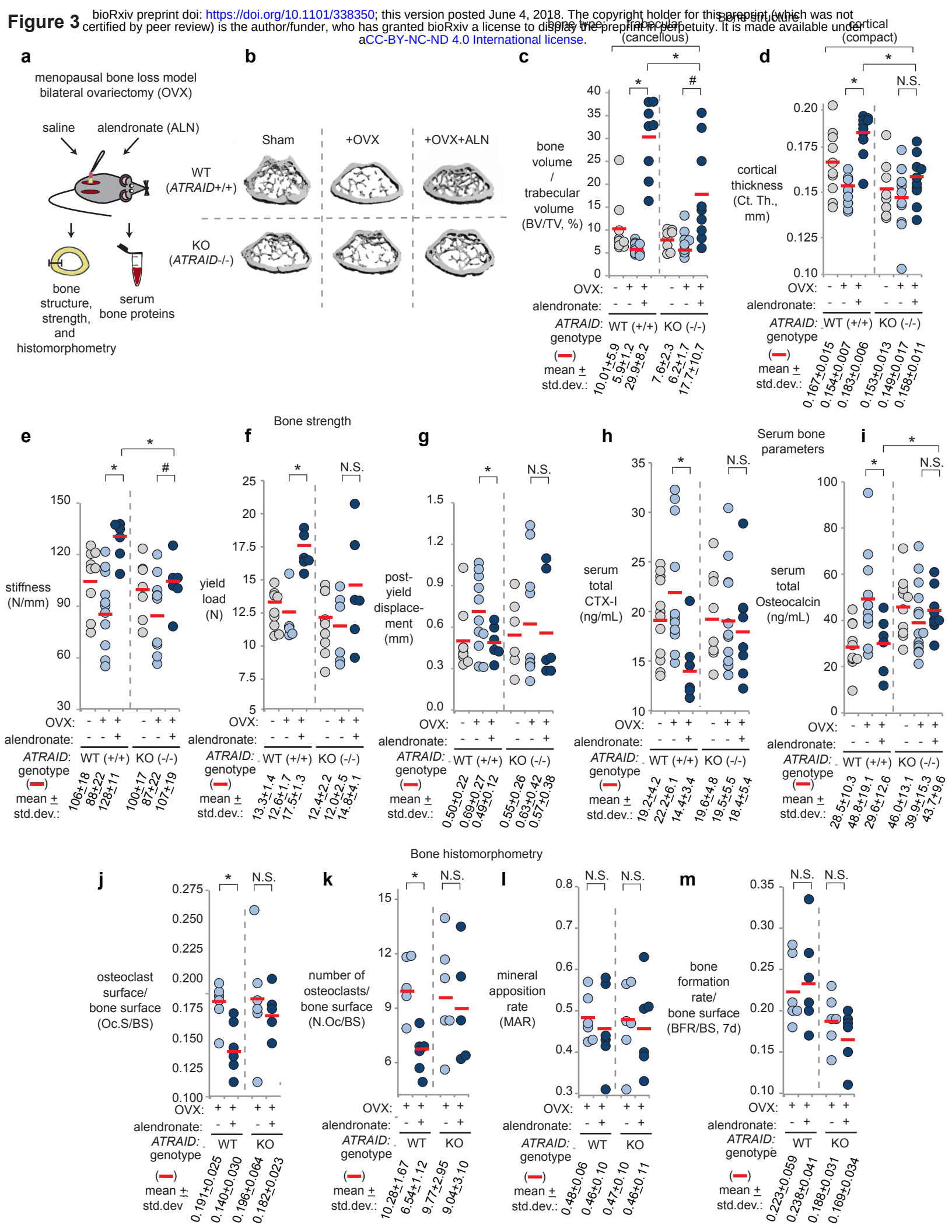

Figure 4

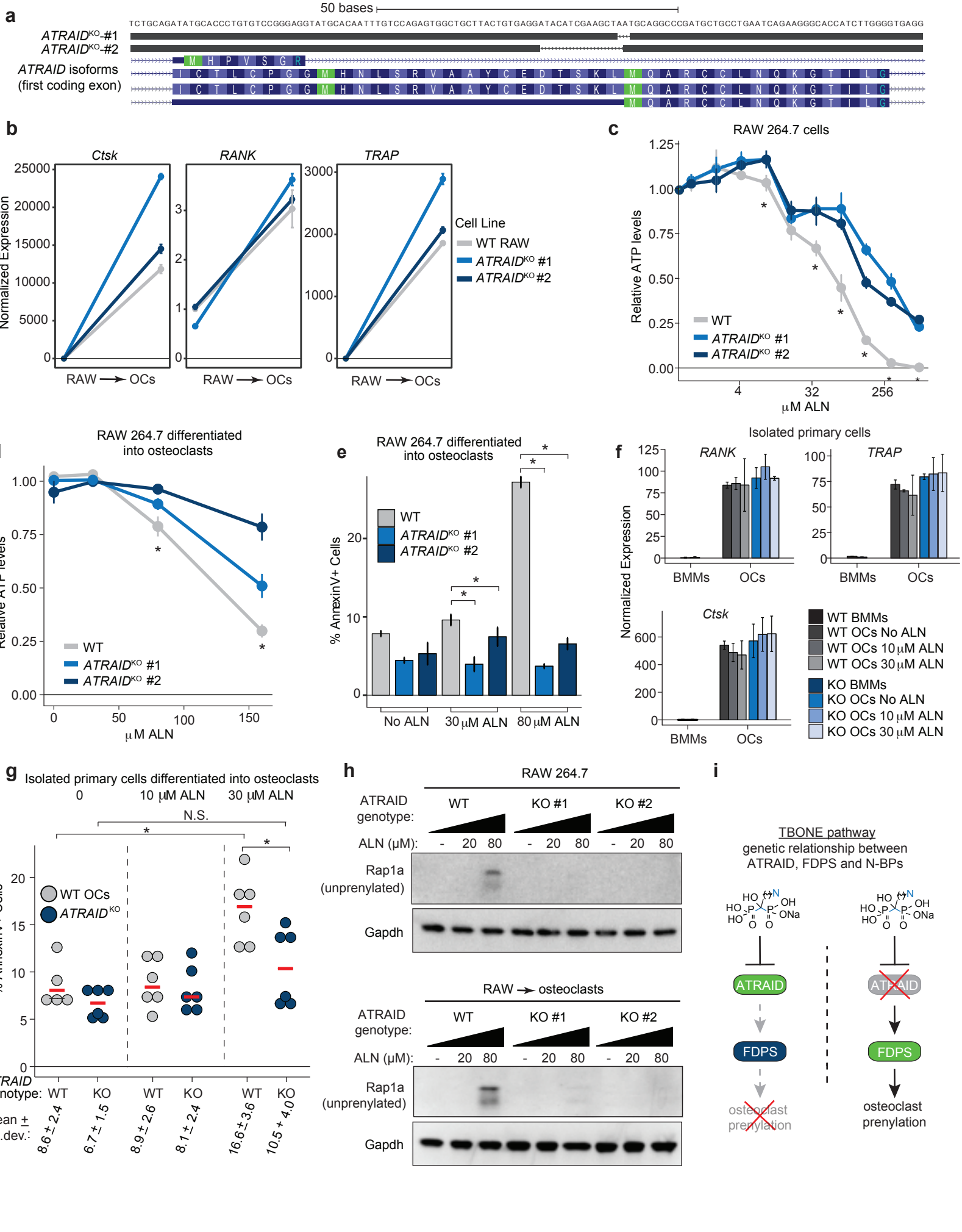

Supplementary Figure 1

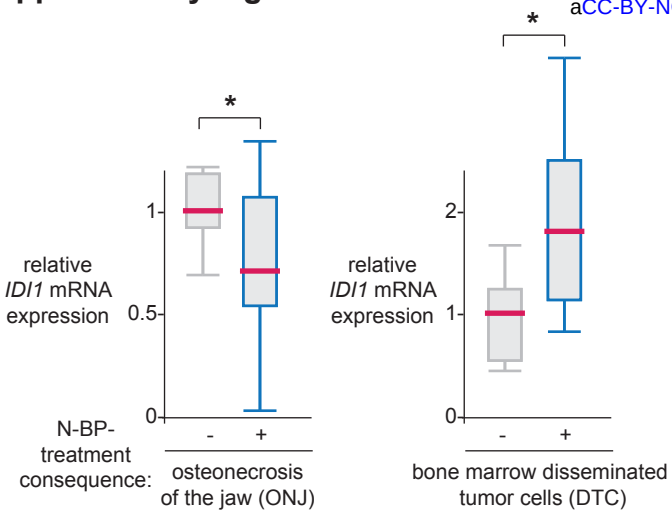

Supplementary Figure 1, related to Figure 1. ATRAID is a genetic factor in responses to N-BPs in cells and in patients.
IDI1 is differentially expressed in multiple myeloma patients who experienced osteonecrosis of the jaw (ONJ) while taking N-BPs and in breast cancer patients whose bone marrow micrometastases, i.e., disseminated tumor cells (DTC), reoccurred or who died <1000 vs. >2500 days after initiating zolendronate treatment. Raw expression values were normalized such that the patients who did not experience the undesirable N-BP treatment outcome had an arbitrary value of 1. * indicates $p < 0.05$. Affymetrix probe for *IDI1*: 204615_x_at.

Supplementary Figure 2

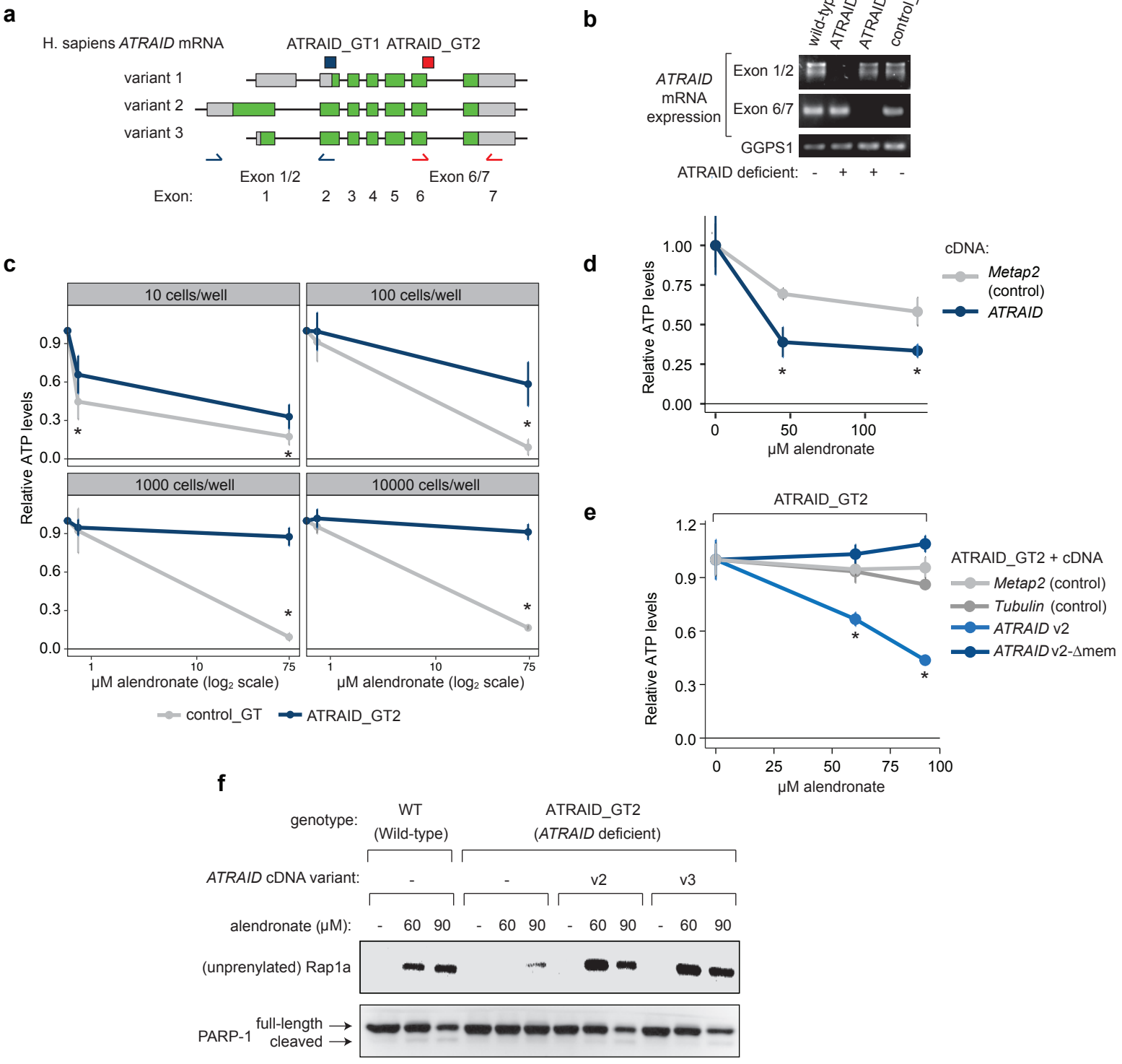

Supplementary Figure 2, related to Figure 2. ATRAID is required for molecular responses to N-BPs.
(a) Schematic of the exon structure of the three human *ATRAID* mRNA variants. The coding sequence for each variant is in green. Non-coding portions of each exon are in grey. The translated regions of variant 1 and variant 3 are shorter than variant 2 due to internal translation initiation sites. The location of the primer sets used to identify each *ATRAID* gene trap (GT) are indicated (in blue for ATRAID_GT1; in red for ATRAID_GT2). **(b)** mRNA analysis of *ATRAID* and *GGPS1* expression levels in clones that contain independent gene-trap insertions in their respective loci. Wild-type KBM7 cells were compared with mutant alleles (labeled as GT) and GGPS1 was used as a loading control. **(c)** *ATRAID*-deficient cells are resistant to alendronate over a wide range of concentrations and cell numbers. KBM7 cell viability was determined by measuring cellular ATP levels and is expressed as a ratio of that compared with untreated cells. All measurements were performed in quadruplicate (biological replicates). * indicates p<0.05, unpaired t-test. **(d)** *ATRAID* overexpression sensitizes cells to alendronate. HEK-293T cells were transfected with either Metap2 (control), or ATRAID-cDNA expressing vectors and the indicated doses of alendronate for 72 hours. Viability measurements were performed in quadruplicate (biological replicates). * indicates p<0.05, unpaired t-test. **(e)** Alendronate regulation of viability is dependent on ATRAID membrane targeting. Cells deficient in *ATRAID* (ATRAID_GT2) were transformed to express exogenous Metap2 (controll), tubulin (control), ATRAID variant 2 (_v2), or ATRAID variant 2 lacking the transmembrane domain (Δmem_v2). Cells were treated with alendronate at the indicated dose for 72 hours. Cell viability was determined as in p<0.05, unpaired t-test (n=6) (3 biological replicates, 3 technical replicates). **(f)** An additional cell line whose alendronate-dependent regulation of prenylation requires *ATRAID*. Wild-type control and *ATRAID*-deficient KBM7 cells exogenously expressing or not expressing *ATRAID* cDNA were treated with the indicated dose of alendronate for 24 hours then lysed and analyzed by immunoblotting for the indicated proteins. Equal amounts of protein were loaded in each lane. This experiment was repeated three times (biological replicates) and was consistent all three times.

Supplementary Figure 3

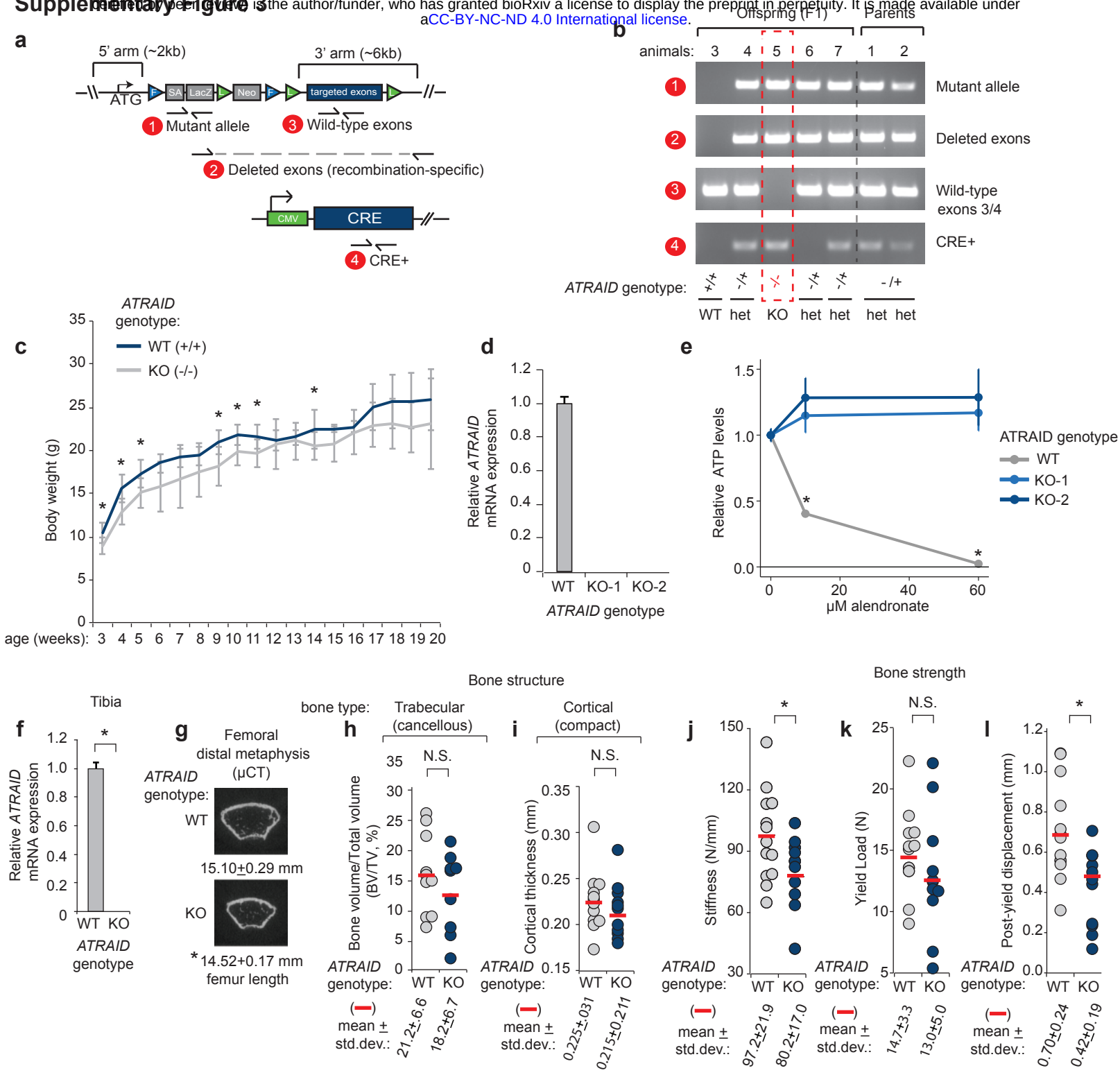

Supplementary Figure 3, related to Figure 3. ATRAID is required for organismal responses to nitrogen-containing bisphosphonates.
(a) Schematic of ATRAID targeted gene locus and genotyping strategy. ATRAID exon 3-exon 5 are targeted, i.e., flanked by LoxP sites. (**b**) Confirmation of deletion of protein-coding genomic DNA at the *ATRAID* gene locus. WT, wild-type at the *ATRAID* locus; het, heterozygous; KO, homozygous deletion. (**c**) *ATRAID* KO mice have reduced body weight compared with *ATRAID* wild-type WT (+/+) mice. N=6-13 for wild-type, N=7-14 for *ATRAID* KO mice. * indicates p<0.05. (**d**) Cells from *ATRAID* KO mice lack *ATRAID* mRNA. Tail fibroblast cells were analyzed for mRNA expression of ATRAID by RT-PCR and normalized to RPLP0 mRNA levels. Error bars indicate standard deviation for n=4 (biological replicates). * indicates p<0.05, unpaired t-test. **(e)** Cells from the tails of *ATRAID* KO animals are resistant to the cytotoxic effects of alendronate. All cells were treated with the indicated concentration of alendronate for 72 hours. Cell viability was determined by measuring cellular ATP levels and is expressed as a ratio of that compared with untreated cells. All measurements were performed in quadruplicate (biological replicates). * indicates p<0.05, unpaired t-test. **(f)** *ATRAID* mRNA is undetectable in tibia of *ATRAID* knockout mice. Tibias were analyzed for *ATRAID* mRNA expression by RT-qPCR and normalized to *RPLP0* mRNA levels. Error bars indicate standard deviation for n=4 (biological replicates). * indicates p<0.05, unpaired t-test. **(g)** Femurs from *ATRAID* KO mice are slightly smaller but morphologically normal. Representative traverse μCT images at the femoral distal metaphysis from wild-type and *ATRAID* KO mice. Femur lengths in millimeters (mm) were based on μCT measurement. Error measurements are standard deviation for n=5-6 mice. * indicates p<0.05, unpaired t-test. (**h, i**) *ATRAID* KO mice bone microstructure isn't significantly altered. Femur trabeculae **(h)** and cortical **(i)** regions were analyzed by μCT. Each circle represents an individual animal. Circles offset to the right represent unique animals with similar values to those of another animal (offset for visual clarity). N=8-10 (2-month-old) mice per group. n.s. indicates not significant, unpaired t-test. **(j-l)** *ATRAID* KO mice have impaired bone strength. Stiffness **(j)**, yield load **(k)**, and post-yield displacement **(l)** were analyzed by three-point bending test. Each circle represents an individual animal. Circles offset to the right represent unique animals with similar values to those of another animal (offset for visual clarity). N=10 mice (2-month-old) per group. * indicates p<0.05, n.s. indicates not significant, unpaired t-test.

Supplementary Figure 3 (continued)

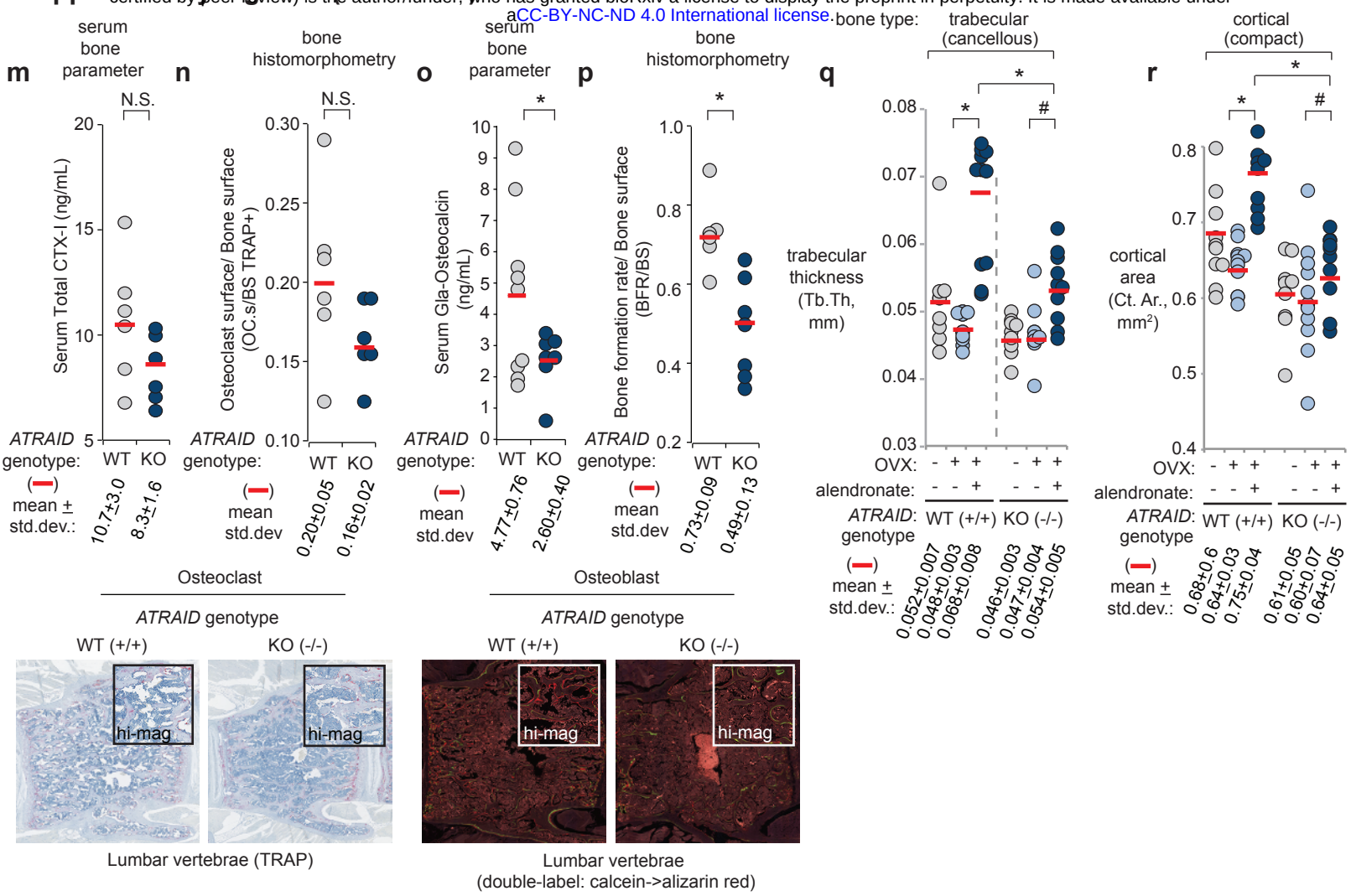

Supplementary Figure 3 (continued), related to Figure 3. ATRAID is required for organismal responses to nitrogen-containing bisphosphonates.
(m,n) Markers of osteoclast function are unchanged comparing *ATRAID* wild-type, WT (+/+) with knockout, KO (-/-) mice. **(m)** Serum C-terminal telopeptides of type I collagen (CTX-I) were measured in serum obtained from 3-month-old males using ELISA. Each circle represents an individual animal. Circles offset to the right represent unique animals with similar values to those of another animal (offset for visual clarity). N=6 mice per group. n.s. indicates not significant, unpaired t-test. **(n)** Osteoclast surface to bone surface ratio (Oc.S/BS) was determined by Tartrate Acid Phosphatase (TRAP)-assay reactivity. Each circle represents an individual animal. Circles offset to the right represent unique animals with similar values to those of another animal (offset for visual clarity). N=6 mice per group. n.s. indicates not significant, unpaired t-test. **(o,p)** *ATRAID* KO mice have altered markers of osteoblast function. **(o)** Gla-Osteocalcin was measured in serum obtained from 3-month-old males using ELISA. Each circle represents an individual animal. Circles offset to the right represent unique animals with similar values to those of another animal (offset for visual clarity). N=7-9 mice per group. * indicates p<0.05, unpaired t-test. **(p)** bone formation rate (BFR/BS) determined by double labeling using calcein followed by alizarin red were analyzed histologically. Each circle represents an individual animal. Circles offset to the right represent unique animals with similar values to those of another animal (offset for visual clarity). N=6-7 mice per group. * indicates p<0.05, n.s. indicates not significant, unpaired t-test. **(q, r)** Ovariectomized *ATRAID* KO mice have impaired bone microstructural responses to alendronate. Femur trabeculae **(q)** and cortical **(r)** regions were analyzed by µCT. Each circle represents an individual animal. Circles offset to the right represent unique animals with similar values to those of another animal (offset for visual clarity). N=8-11 mice (3.5-month-old) per group. * indicates p<0.01, #indicates 0.01<p<0.05..

Supplementary Figure 4

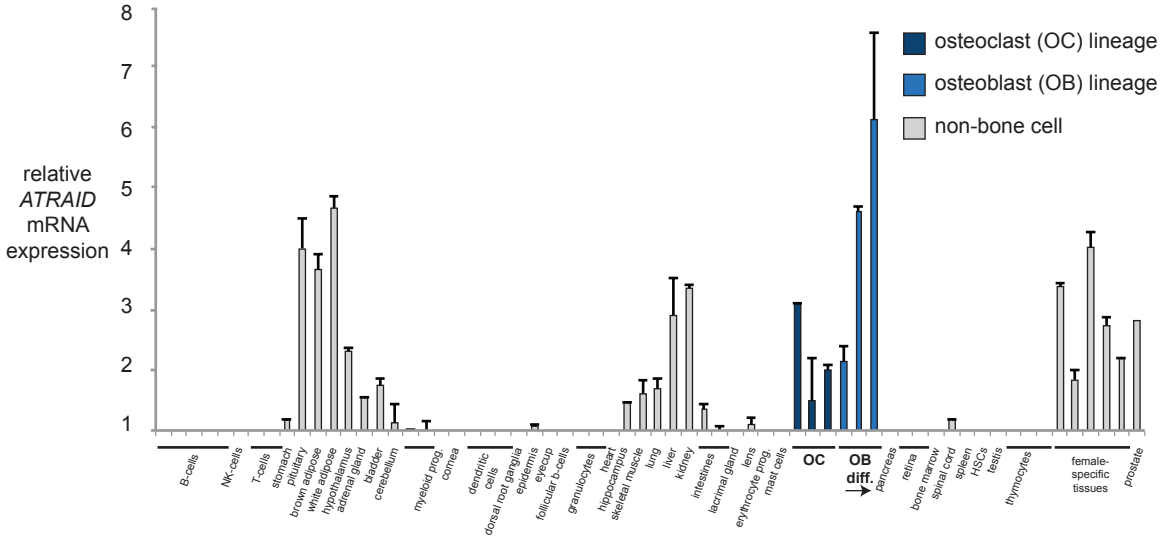

Supplementary Figure 4, related to Figure 4. ATRAID is required for the effects of alendronate on osteoclasts.
ATRAID expression in mouse tissues and cell lines. Affymetrix microarray data using probe 1428380_at was obtained from BIOGPS. Female-specific tissues include umbilical cord, mammary glands, ovaries, uterus, placenta. Error bars indicate standard error for pools of tissue from 4 male, 3 female mice with 2 technical replicates.